frontiers | Frontiers in Earth Science

TYPE Original Research
PUBLISHED 06 October 2023
DOI 10.3389/feart.2023.1251953

OPEN ACCESS

EDITED BY
Wei-Qiang Ji,
Chinese Academy of Sciences (CAS), China

REVIEWED BY
Gaoxue Yang,
Chang'an University, China
Xiao-Qing Zhu,
Qingdao Institute of Marine Geology (QIMG), China

*CORRESPONDENCE
Zhongbo Wang,
zhbwang@stu.edu.cn

RECEIVED 04 July 2023
ACCEPTED 21 September 2023
PUBLISHED 06 October 2023

CITATION
Liu Y, Fang N and Wang Z (2023), The geochemical characteristics of Cretaceous volcanics in southern Hainan Island and implications for tectonic evolution in the South China Sea. *Front. Earth Sci.* 11:1251953. doi: 10.3389/feart.2023.1251953

The geochemical characteristics of Cretaceous volcanics in southern Hainan Island and implications for tectonic evolution in the South China Sea

Yang Liu[1], Nianqiao Fang[2] and Zhongbo Wang[1,3]*

[1]Guangdong Provincial Key Laboratory of the Marine Disaster Prediction and Prevention, Institute of Marine Sciences, Shantou University, Shantou, China, [2]School of Ocean Sciences, China University of Geosciences, Beijing, China, [3]Laboratory for Marine Mineral Resources, Pilot National Laboratory for Marine Science and Technology, Qingdao, China

The southeastern Eurasian plate, where the South China Sea (SCS) is located, lies in a complex tectonic setting between the Pacific and Tethys tectonic belts. It is widely accepted that the tectonics of the SCS area were influenced by subduction in the late Mesozoic, but there is still controversy over whether it was paleo-Pacific subduction or Tethyan subduction. Volcanic activity in the south of Hainan Island was intense during the Cretaceous, and geochemical analysis of the collected basaltic andesite, andesite and rhyolite samples in this study indicate those intermediate-acid series igneous rocks are high-K calc-alkaline or calc-alkaline. Some andesites have high MgO contents and $Mg^{\#}$ values (2.04–5.34 wt% and 36.83–55.29; $Mg^{\#} = 100\times Mg^{2+}/(Mg^{2+} + TFe^{2+})$. Light rare earth elements (LREEs) and large ion lithophile elements (LILEs) are enriched in all the samples, but high field strength elements (HFSEs) are depleted. The negative Eu anomalies are more obvious in the rhyolites than andesites. The geochemical characteristics of the volcanic arc igneous rocks show that the mid-Cretaceous tectonic setting of Hainan Island can be classified as an Andean active continental margin. During the mid-Cretaceous, intermediate volcanism occurred in Hainan Island and its adjacent areas. The zircon-saturation temperatures of the acid volcanic rocks in study area exhibit relatively low values (ranging from 746°C–790°C). Unlike igneous rocks forming in the coastal area east of the South China Block at the same time, no A-type granitoids with alkaline dark minerals appear in Hainan Island. During the late Mesozoic, the western SCS, where Hainan Island was located, may not have been affected by the subduction of the paleo-Pacific Plate, but rather Neotethyan subduction which dominated the Cretaceous magmatic and tectonic activities along the western margin of the SCS. This finding helps to understand the late Mesozoic tectonic evolution of the southeastern edge of the Eurasian plate.

KEYWORDS

andesites, rhyolites, geochemical characteristics, active continental margin, Neotethyan subduction

1 Introduction

The southeastern Eurasian Plate lies among the Pacific Plate, Philippine Sea Plate and the India-Australia Plate (Figure 1A), and between the circum-Pacific belt and the Tethys belt, which implies a complicated tectonic evolution. The Cenozoic opening and growth of the South China Sea (SCS) is a remarkable tectonic event in this region. However, there are many disputes regarding the tectonics of this area before the opening of the SCS and the extension of the continental margin of the South China Block (SCB). In the late

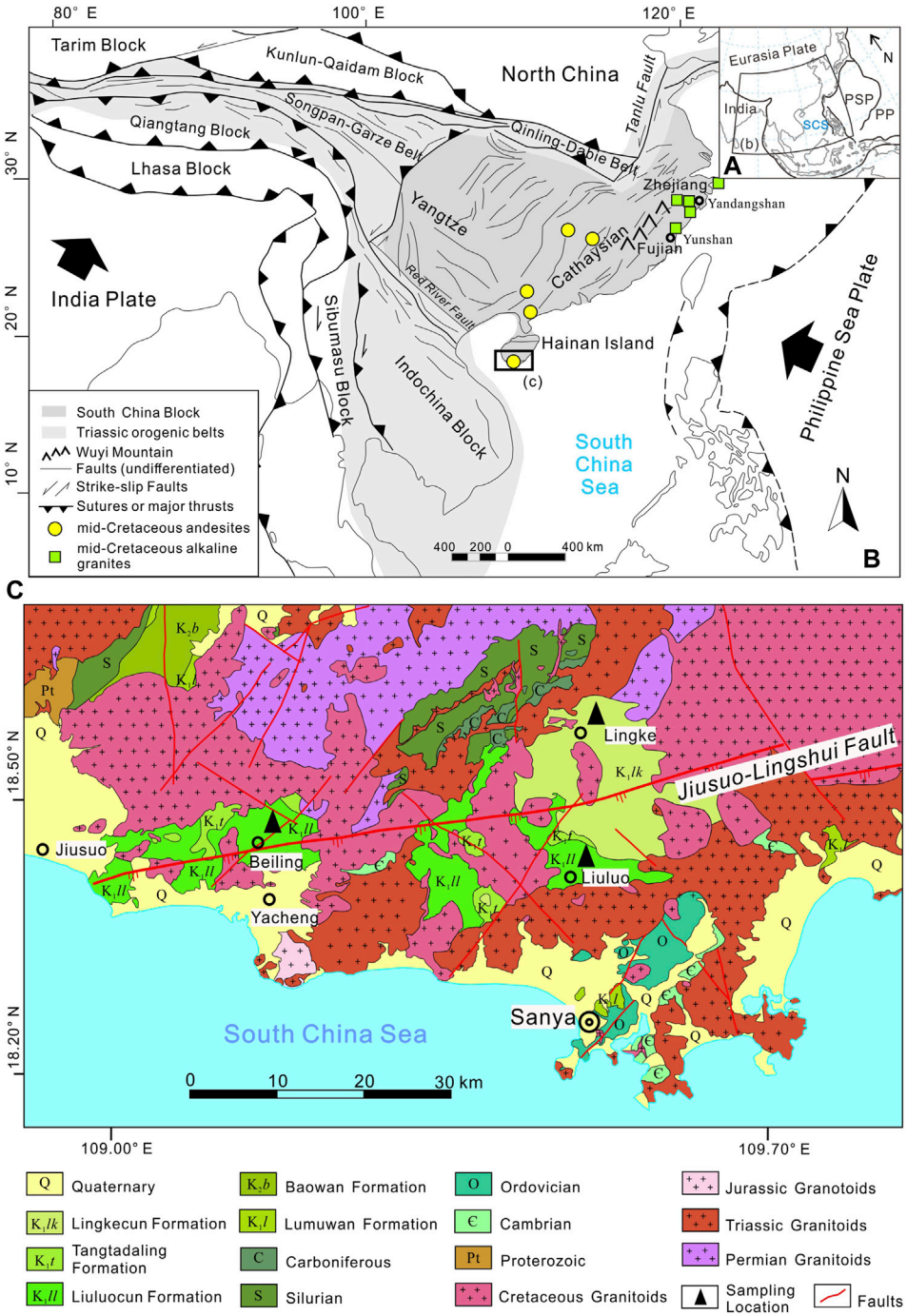

FIGURE 1
(A) The location of the South China Sea relative to surrounding tectonic plates (modified from Yin, 2010); **(B)** sketched structural map of Southeast Asia showing the location of Hainan Island and its tectonic subdivision in the South China Sea (modified from Li et al., 2016); and **(C)** geological map of southern Hainan Island (modified from Zhou et al., 2015a; Cai and Fu, 1997). Annotations: The South China Block is surrounded by North China Block, the western Tibet Plateau, the southwest Sibumasu-Indochina Block, and the Philippine Sea Plate. The black arrows show the directions of the Pacific and India Plate drift. The Jiusuo-Lingshui Fault is a southward dipping thrust fault located in southern Hainan Island (Figure 1C). SCS, South China Sea; PSP, Philippine Sea Plate; PP, Pacific Plate.

Mesozoic, this region is often regarded as the southwestern extension of the magmatic belt of the eastern SCB, followed by a transition from the Tethys orogenic regime to the paleo-Pacific tectonic regime (Zhou and Li, 2000; Wang et al., 2001; Xia and Zhao, 2014; Zhou et al., 2015a; Zahirovic et al., 2016). Because of the subduction and rollback of the paleo-Pacific Plate, the western margin of the SCS experienced a regional lithospheric extension, and large-scale magmatism occurred in this region (Li et al., 1999; Thuy et al., 2004; Geng et al., 2006; Yan et al., 2010; Wang et al., 2012; Wang et al., 2019; Tang et al., 2014; Zhou et al., 2015a; Xu et al., 2016; Sun et al., 2017; Yan et al., 2017; Nong et al., 2021; Yang et al., 2022). On the other hand, some studies suggest that tectonic and magmatic activities with related ore deposits were still affected by the Tethys orogenic regime during the Cretaceous (Fang, 2016; Sun, 2016; Zhang et al., 2017; Zhu et al., 2017; Sun et al., 2018; Huang et al., 2019; Yuan et al., 2019; Liu et al., 2020; 2021). The debates over which subduction affected the SCS have led to differences in the identification of geological features on the southeastern Eurasian Plate during the late Mesozoic, such as magmatic activities and mineralization.

Cretaceous granitoids were extensively studied to explore tectonic evolution during the Mesozoic period because of their numerous outcrop areas (Li et al., 1999; Thuy et al., 2004; Yan et al., 2010; Wang et al., 2012; 2019; Tang et al., 2014; Xu et al., 2016; Sun et al., 2017; Yan et al., 2017; Zhang et al., 2017; Zhu et al., 2017; Sun et al., 2018; Huang et al., 2019; Yuan et al., 2019; Nong et al., 2021), which implies these studies give less consideration of other magmatic rocks, such as andesites, from this period. Considering the region where the SCS lies was an active continental margin, the volcanic rocks need to be studied comprehensively, especially intermediate rocks, which will help to better understand the state of the lithosphere and deep mantle, and the tectonic setting of this region.

Located in the northwestern SCS, Hainan Island has a large outcrop of Cretaceous volcanic rocks and is one of the most important exposed areas of Cretaceous andesite on the SCB. Therefore, a detailed study of the Cretaceous volcanic rocks in Hainan Island will help to characterize the type of volcanic activity along the margin of the SCS during the Cretaceous period, and improve our understanding of the tectonic evolution of the southeast edge of the Eurasian plate during the late Mesozoic.

2 Geological setting and sample information

Hainan Island, located at the intersection of the Eurasian, Indian-Australian, Philippine Sea and Pacific plates, is separated from the Chinese mainland by the Qiongzhou Strait (Figure 1B). Hainan Island has experienced multi-stage tectonic movements, and an E-W trending tectonic system is the main structural system. The Baoban Group, about 1.43 Ga (Li et al., 2008), is the oldest known basement exposed on the island. The strata outcrop on Hainan Island is very limited, accounting for only 18.6% of the island area, and the remaining area generally has magmatic rocks (Figure 1C), especially granitoid rocks covering ca. 40% area of the island (Zhou et al., 2015b).

Extensive Cretaceous volcanism resulted in a >5200 m thick volcanic sequence, which is divided, from the base to the top, into the Liuluocun, Tangtadaling and Lingkecun formations (Guangdong BGMR, 1988). The rocks consist predominantly of intermediate-felsic compositions, with minor occurrences of mafic volcanic rocks, and are primarily distributed along the Jiusuo-Lingshui Fault, a southward dipping thrust fault located in southern Hainan Island (Figure 1C). The Liuluocun Formation consists of rhyolitic tuff lava, flow-banded rhyolite on the top, rhyolitic ignimbrite, eruptive breccia with stratified basalt, and andesite in the lower part and purplish red siliciclastic rock at the bottom. The Liuluocun Formation is unconformably overlain by the Tangtadaling Formation, which is mainly composed of dacitic tuff. The Lingkecun Formation, on the top of this volcanic sequence, is mainly composed of rhyolitic lava and pyroclastic rocks, with several layers of dacites. According to zircon geochronology, rhyolitic and andesitic rocks of the Liuluocun Formation formed in 107–101.5 Ma, and the age of the Lingkecun Formation was about 98 Ma (Cai and Fu, 1997; Zhou et al., 2015a). The Cretaceous magmatic activities in the south of Hainan Island occurred about the mid-Cretaceous (110–90 Ma) (Tang et al., 2010; Sun et al., 2018; Yuan et al., 2019).

The samples were collected from Beiling, Liuluo and Lingke, respectively. The Liuluocun Formation was sampled in Beiling and Liuluo, while the Lingke samples were from the Lingkecun Formation (Figures 2A, B). Based on hand specimens, these samples are andesite or rhyolite. Andesite samples are dark gray in color, massive, and porphyritic (Figures 2C, E, G). Andesites from Beiling and Liuluo contain 10%–30% phenocrysts, of which are mostly plagioclase with minor amounts of dark minerals. The dark minerals are mainly hornblende with a small amount of pyroxene (Figures 2C, E). But phenocrysts of andesites from Lingke are much less common (~10%), and they are all pyroxene (Figure 2G). Dark minerals have been altered to chlorite. The matrix of andesites consists of microcrysts of plagioclase, dark minerals, Fe-Ti oxides, zircon and apatite.

Rhyolite samples are light purple or gray in color, massive, and porphyritic (Figures 2D, F, H). The phenocrysts include quartz (10–15 vol%), plagioclase (3-8 vol%), alkali feldspar (5–10 vol%) and biotite (~3%). Those phenocrysts are slightly altered. Chalcedony can be seen in some rhyolites (Figure 2F). The matrix consists of microcrysts and opaque minerals.

3 Methods

The samples were ground to 74-μm using an agate mortar and pestle. To determine the oxides of major elements, samples were analyzed according to the Chinese National Standard GB/T14506.28-2010 (National Standard of P.R. China, 2011b). About 0.7 g of powder and 7 g of latent solvent ($Li_2B_4O_7$ + LiF + NH_4NO_3) were weighed out and stirred together in a Pt-(Au) crucible. Then, 1 mL BrLi was added in the crucible at 1200°C for 20 min. The liquid melt was used to make a matrix for analysis. About 1 g sample was added in a crucible (W_1) and weighed (W_2). The crucible was placed in a muffle furnace at 1000°C for 2 h and then dried and weighed (W_3). The loss on ignition (LOI) was determined using the following equation:

$$LOI = (W_2 - W_3) / (W_2 - W_1)$$

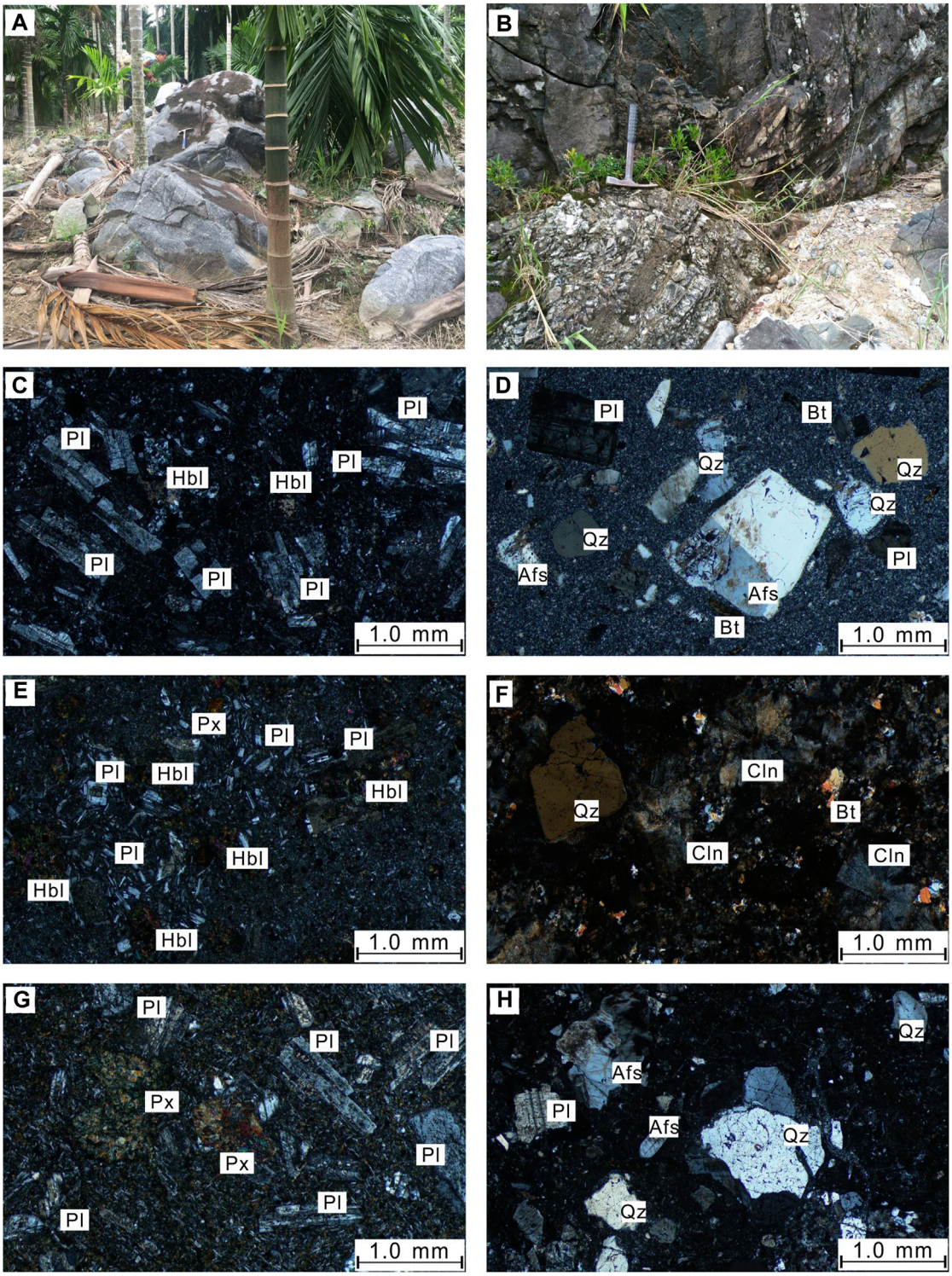

FIGURE 2
Field photograph **(A, B)** and photomicrographs **(C–H)** of Cretaceous volcanic rocks from southern Hainan Island. Annotations: **(A, C, D)** from Beiling; **(E, F)** from Liuluo; **(B, G, H)** from Lingke. **(C–F)** from Liuluo Formation; **(G, H)** from Lingkecun Formation. **(C, E, G)** andesitic samples; **(D, F, H)** rhyolitic samples. Abbreviations: Pl, plagioclase; Hbl, hornblende; Px, pyroxene; Qtz, quartz; Afs, alkali feldspar; Bt, biotite; Cln, Chalcedony.

Major element oxides except FeO were analyzed on fused glass discs using a Rikagu RIX 2100 X-ray fluorescence spectrometer (XRF). FeO contents were analyzed by wet chemical analysis based on the National Standard of P.R. China (2011a). The Chinese national reference material GBW07104 was used for quality control. The method detection limit (MDL) for each element was calculated as three times the standard deviation of the average from the blank samples (n = 10). The uncertainties of major element analyses were better than ±5%.

10.3389/feart.2023.1251953

TABLE 1 Major element (wt%) and trace element (ppm) compositions of the Cretaceous volcanic rocks of southern Hainan Island.

Samples	Beiling								Liuluo			Lingke			
	BLRR1	BLRR501	16SY05-3R	16SY06-1	BLRR201	16SY01-2	16SY03-2	16SY06-5	16SY10-6-1	16SY10-5-1	16SY10-2	16SY08-3-1	16SY08-2	16SY08-1	16SY08-5-1
SiO_2	52.90	56.73	55.31	59.64	68.20	76.04	78.14	71.52	57.56	55.65	77.38	53.84	53.35	75.41	72.41
Al_2O_3	16.63	18.17	19.00	17.52	15.92	12.78	11.95	14.12	17.65	19.40	12.37	17.22	17.01	12.41	14.30
TiO_2	1.13	0.88	1.06	0.81	0.45	0.16	0.07	0.32	0.71	0.92	0.10	0.97	0.99	0.15	0.30
Fe_2O_3	2.74	5.81	4.74	5.00	2.52	0.48	0.71	1.19	3.25	3.13	0.53	1.86	1.89	0.63	1.32
FeO	4.65	1.99	3.35	1.73	0.57	0.76	0.39	1.22	2.75	2.92	0.18	6.02	6.08	0.91	1.02
CaO	7.47	5.80	7.54	5.47	2.03	1.02	0.80	2.06	8.65	7.52	0.70	8.04	8.33	0.93	0.23
MgO	4.88	3.04	2.81	2.04	0.71	0.28	0.27	0.74	3.25	2.66	0.09	5.34	5.24	0.49	1.63
K_2O	2.73	1.38	0.94	2.49	4.35	4.64	2.69	5.06	1.96	2.77	5.43	1.70	1.88	5.12	4.41
Na_2O	2.48	3.01	3.14	3.02	3.05	3.40	4.05	2.61	2.14	3.00	2.70	2.85	2.87	3.06	2.19
MnO	0.16	0.13	0.16	0.10	0.05	0.06	0.07	0.11	0.15	0.16	0.02	0.15	0.13	0.05	0.11
P_2O_5	0.54	0.29	0.26	0.25	0.12	0.03	0.04	0.09	0.32	0.36	0.01	0.27	0.27	0.03	0.02
LOI	3.45	2.61	1.52	1.77	1.86	0.31	0.73	0.85	1.41	1.28	0.42	1.59	1.78	0.75	1.98
Total	99.73	99.84	99.82	99.84	99.84	99.96	99.91	99.86	99.81	99.78	99.94	99.85	99.84	99.94	99.92
A/CNK	0.60	0.99	1.61	1.43	1.50	8.48	4.81	2.49	1.14	1.66	5.99	1.42	1.31	3.70	1.04
FeO*	7.11	7.22	7.61	6.24	2.84	1.19	1.03	2.29	5.68	5.74	0.65	7.69	7.79	1.48	2.21
$Mg^{\#}$	55.01	42.85	39.65	36.83	30.65	29.65	31.94	36.46	50.54	45.21	20.45	55.29	54.56	37.12	56.69
La	46.13	30.45	26.1	32.0	55.04	30.6	39.9	54.9	28.0	24.7	28.1	24.3	30.5	42.1	20.2
Ce	91.44	56.98	55.8	56.0	88.14	60.1	65.9	88.7	48.1	54.2	48.5	43.5	48.9	83.1	31.1
Pr	12.06	7.28	6.76	6.76	11.46	6.59	7.38	10.9	5.98	6.70	5.66	5.55	6.14	9.82	3.74
Nd	48.18	28.56	27.5	26.8	40.56	23.6	25.4	40.8	24.3	28.1	19.3	23.2	26.2	37.3	14.2
Sm	9.12	5.64	5.32	5.11	6.98	4.71	4.04	7.59	4.17	5.46	3.37	4.63	5.29	7.08	2.73
Eu	2.50	1.71	1.51	1.30	1.51	0.37	0.76	1.52	1.24	1.68	0.43	1.27	1.43	0.49	0.52
Gd	7.75	5.16	4.61	4.50	6.02	4.48	3.94	7.19	3.57	4.62	3.29	4.14	4.67	6.12	2.62
Tb	1.11	0.82	0.70	0.71	0.88	0.76	0.52	1.11	0.53	0.69	0.48	0.68	0.74	0.90	0.47
Dy	5.89	4.86	3.82	3.96	5.04	4.81	2.73	6.27	2.88	3.62	2.81	4.02	4.06	4.96	3.13

(Continued on following page)

TABLE 1 (*Continued*) Major element (wt%) and trace element (ppm) compositions of the Cretaceous volcanic rocks of southern Hainan Island.

Samples	Beiling								Liuluo			Lingke			
	BLRR1	BLRR501	16SY05-3R	16SY06-1	BLRR201	16SY01-2	16SY03-2	16SY06-5	16SY10-6-1	16SY10-5-1	16SY10-2	16SY08-3-1	16SY08-2	16SY08-1	16SY08-5-1
Ho	1.08	0.94	0.67	0.72	0.95	0.95	0.50	1.13	0.53	0.64	0.53	0.73	0.71	0.92	0.63
Er	2.89	2.43	1.87	2.04	2.60	2.93	1.52	3.18	1.48	1.76	1.65	1.93	1.99	2.80	1.89
Tm	0.45	0.41	0.32	0.34	0.46	0.51	0.24	0.48	0.23	0.30	0.28	0.29	0.33	0.43	0.30
Yb	2.51	2.39	1.99	2.12	2.83	3.36	1.60	2.99	1.41	1.87	1.83	1.79	2.07	2.76	1.87
Lu	0.57	0.50	0.28	0.30	0.55	0.57	0.27	0.49	0.23	0.27	0.31	0.28	0.30	0.47	0.31
Y	33.53	27.08	24.6	26.9	25.30	27.0	15.6	31.4	15.1	22.2	16.9	19.7	23.8	25.0	20.6
Ba	879.3	792.8	523	559	1062	159	411	666	671	844	275	347	402	232	346
Rb	57.2	52.0	39.0	89.8	162.2	256	83.1	157	54.0	81.0	196	57.8	57.6	192	251
Th	6.99	5.28	4.43	3.99	19.64	29.2	16.4	20.2	2.73	2.48	20.8	4.37	3.68	21.0	11.2
Nb	14.46	12.81	12.7	12.8	11.00	22.4	14.1	12.9	13.3	14.4	16.0	12.2	10.3	16.5	11.4
U	1.84	1.55	0.87	1.74	5.28	11.2	5.36	4.59	0.83	1.23	4.63	1.07	1.16	4.42	2.33
Ta	0.85	0.86	0.59	0.77	1.29	2.23	1.22	0.99	0.48	0.92	1.70	0.48	1.22	1.36	1.04
Sr	924.6	652.5	700	581	411.7	76.5	151	318	788	790	77.8	690	576	103	49.6
Pb	18.1	17.0	12.51	15.97	24.0	25.4	25.1	24.7	7.84	16.21	23.8	13.3	14.67	12.5	12.9
Zr	254.0	164.1	172	176	152.1	102	115	149	151	196	89.9	145	173	143	131
Hf	7.25	4.56	4.82	5.29	8.39	3.81	3.74	4.08	4.22	5.77	3.61	4.13	5.29	5.19	4.11
Cr	74.3	9.4	18.9	3.05	11.8	3.60	4.98	5.02	23.4	32.7	2.67	111	101	6.69	9.41
Ni	49.8	6.8	7.10	2.15	3.9	0.55	0.99	1.97	14.9	12.6	0.41	44.8	38.8	2.68	5.65
Ga	20.29	24.00	23.9	20.9	19.44	14.9	7.95	16.2	20.9	24.0	11.5	19.6	20.8	15.3	17.9
∑REE	231.67	148.12	137.15	142.60	223.02	144.38	154.68	227.23	122.58	134.53	116.54	116.25	133.31	199.36	83.74
LREE/HREE	3.76	2.93	3.16	3.08	4.56	2.78	5.32	3.77	4.31	3.36	3.76	3.05	3.06	4.05	2.28
$(La/Yb)_N$	13.19	9.14	9.38	10.84	13.94	6.53	17.90	13.16	14.28	9.47	11.00	9.75	10.56	10.94	7.76
δEu	0.89	0.95	0.91	0.81	0.69	0.24	0.57	0.62	0.96	0.99	0.39	0.87	0.86	0.22	0.59
Sr/Y	27.58	24.10	28.46	21.64	16.27	2.83	9.63	10.14	52.36	35.65	4.60	34.96	24.18	4.12	2.40

10.3389/feart.2023.1251953

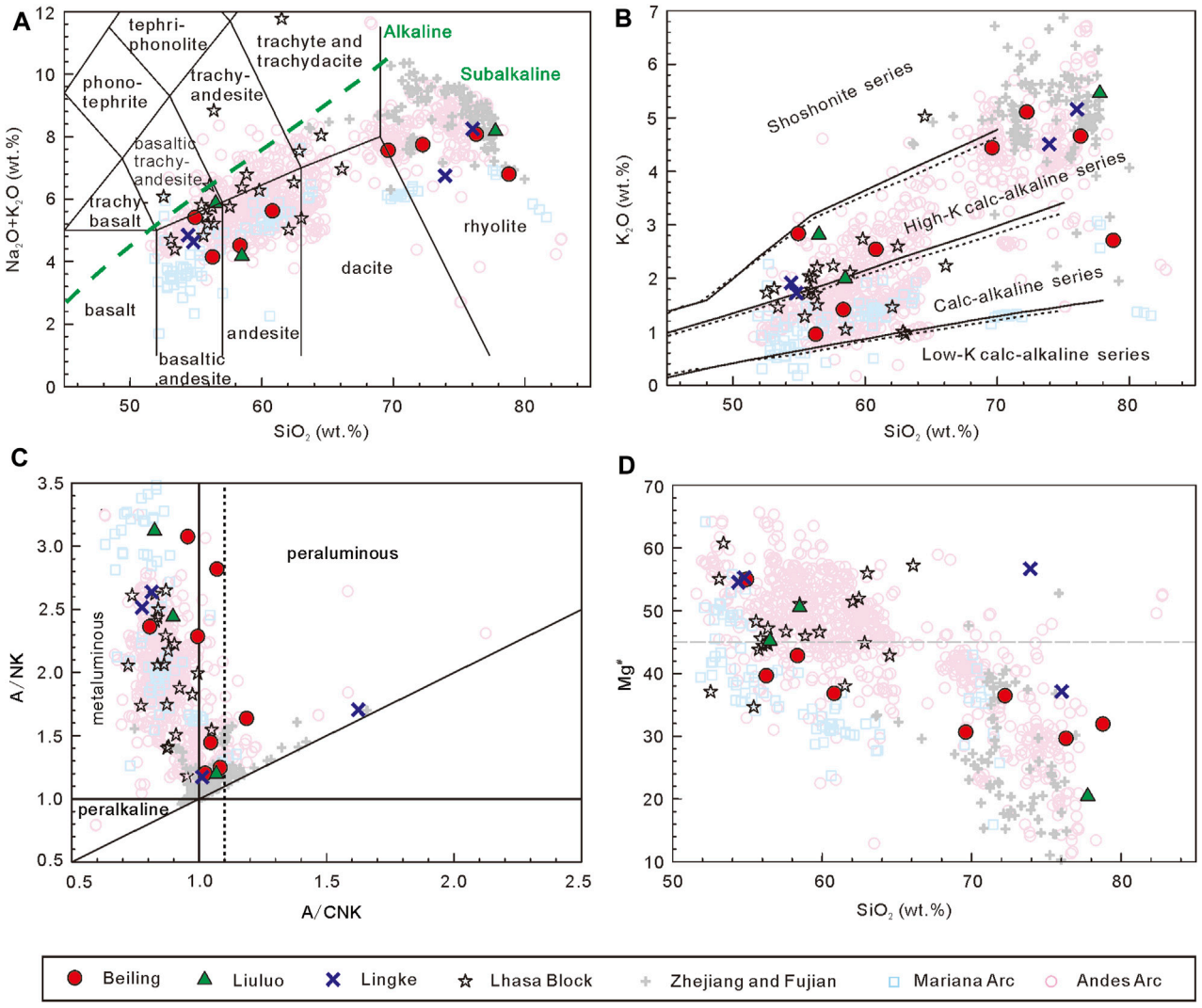

FIGURE 3
Geochemical classification diagrams for Cretaceous volcanic rocks from southern Hainan Island: **(A)** (Na_2O+ K_2O) vs. SiO_2 diagram (after Le Bas et al., 1986). The green line separating alkaline and sub-alkaline igneous rocks is taken from Irvine and Baragar (1971); **(B)** SiO_2 vs. K_2O diagram (after Peccerillo and Taylor, 1976); **(C)** A/NK vs. A/CNK diagram (after Maniar and Piccoli, 1989). A/NK: molar Al_2O_3/[K_2O+ Na_2O]; A/CNK: molar Al_2O_3/[CaO +K_2O+ Na_2O]; and **(D)** $Mg^{\#}$ vs. SiO_2 diagram. Annotations: The geochemical data of mid-Cretaceous volcanic rocks in the Lhasa Block are from Ran et al. (2019) and Zhang et al. (2019a). The geochemical data of those in Zhejiang and Fujian are from Lapierre et al. (1997), Qiu. et al. (1999a), Yu et al. (2008), Hong (2012), Hong et al. (2013), Yan et al. (2016), Yan et al. (2018), and Li et al. (2017). The geochemical data of volcanic rocks in the Andes Arc are from Tormey et al. (1995), Kay et al. (2005), Mamani et al. (2008), Mamani et al. (2009), Schiano et al. (2010), Folkes et al. (2011), Garrison et al. (2011), Pistolesi et al. (2015), Anderson et al. (2017), and Bablon et al. (2020). The geochemical data of volcanic rocks in the Mariana Arc are from Dixon and Batiza (1979), Hole et al. (1984), Bloomer et al. (1989), Lin et al. (1989), Woodhead (1989), Elliott et al. (1997), Wade et al. (2005), Reagan et al. (2008), Marske et al. (2010), Stern et al. (2013), Stern et al. (2019), and Klaver et al. (2020).

The sample preparation for trace element analysis was according to the National Standard of P.R. China GB/T14506.30-2010 (2011). Powdered samples of about 50 mg were weighed and then dissolved in HNO_3 (0.5 mL)-HF (1 mL) in Teflon bombs at 185°C for 24 h, dried, and then treated with HNO_3 (0.5 mL). All samples underwent acid digestion twice and were then treated with HNO_3 (5 mL) at 130°C for 3 h. Dissolved samples were diluted to 50 mL in a clean PET bottle prior to the analyses. ^{103}Rh and ^{185}Re were used as the internal standard references. The trace elements were measured using an Agilent 7500a inductively coupled plasma mass spectrometer (ICP-MS). The precision of all trace elements was estimated to be ±10%.

Major and trace elements of the samples were analyzed at the Hebei Institute of Geology and Mineral Resources, China Geological Survey.

4 Results

Major and trace element data for the mid-Cretaceous volcanic rocks in southern Hainan Island are presented in Table 1. In the Na_2O+K_2O vs. SiO_2 diagram (Figure 3A), volcanic samples fall within the basaltic andesite-andesite-rhyolite field. The andesite/basaltic andesite samples are characterized by relatively low SiO_2,

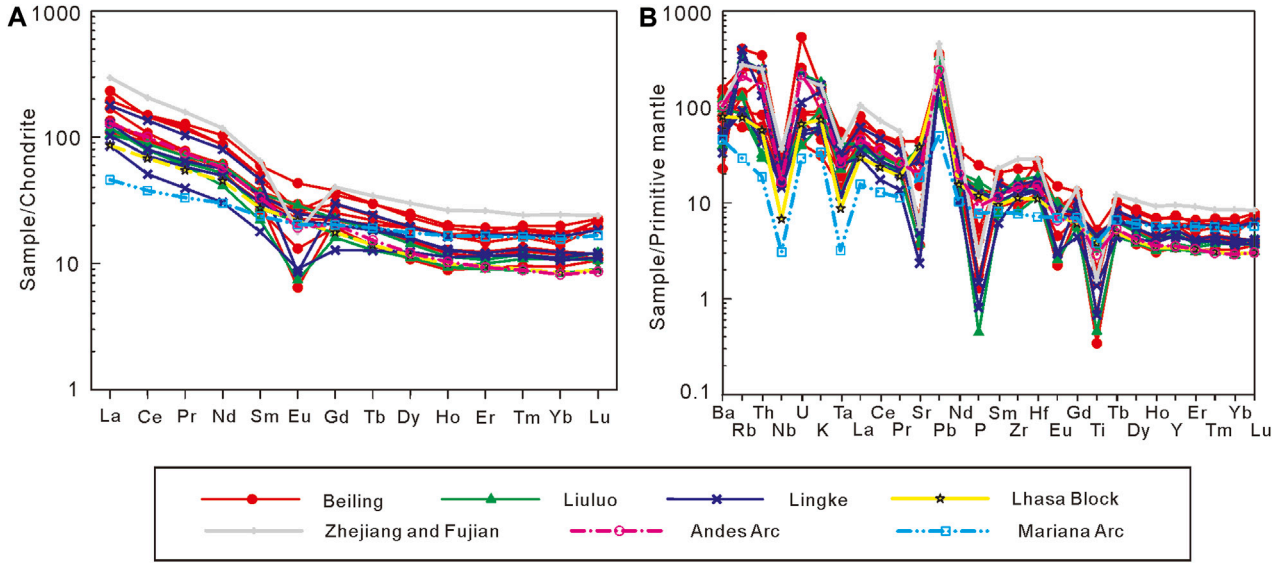

FIGURE 4
(A) Chondrite-normalized REE patterns and **(B)** primitive mantle-normalized trace element spider diagrams for Cretaceous volcanic rocks from southern Hainan Island. Normalizing values are taken from Sun and McDonough (1989). The REE and trace element data of the Lhasa Block, Zhejiang-Fujian, the Andes Arc and the Mariana Arc are shown as average values.

Na_2O and K_2O contents (52.90–59.64 wt%, 2.14–3.14 wt% and 0.94–2.77 wt%). Some basaltic andesites and andesites display elevated MgO contents as well as high $Mg^{\#}$ values [$Mg^{\#}$ = 100× $Mg^{2+}/(Mg^{2+}$ + $TFe^{2+})$]. Thus, they can be classified as high-Mg andesite according to Kelemen (1995) (54–65 wt% SiO_2; >45 $Mg^{\#}$ values) (Figure 3D). The rhyolites posses relatively high SiO_2, Na_2O and K_2O contents (68.20–78.14 wt%, 2.19–4.05 wt% and 2.69–5.43 wt%). The moderate K_2O content suggests that the volcanics are calc-alkaline or high-K calc-alkaline (Figure 3B). Relatively high Al_2O_3 contents (12.05–19.70 wt%) with elevated A/NK values (1.20–3.12; A/NK = molar $Al_2O_3/[K_2O+ Na_2O]$) and moderate A/CNK values (0.81–1.62; A/CNK = molar $Al_2O_3/[CaO + K_2O+ Na_2O]$) indicate mid-Cretaceous volcanics are metaluminous to peraluminous (Figure 3C). These samples exhibit a geochemical composition similar to the volcanic rocks from the Andes Arc.

The volcanic samples have total rare earth element (ΣREE) contents ranging from 83.70 ppm to 231.70 ppm, and obvious fractionation between light and heavy REEs with $(La/Yb)_N$ values of 6.53–17.90 (Table 1; Figure 4A). The chondrite-normalized REE patterns show variable negative Eu anomalies. The δEu values [$\delta Eu = 2\times Eu_N/(Sm_N+Gd_N)$] range from 0.99 to 0.22 as a result of plagioclase fractionation, while the Eu anomalies of the rhyolites are more negative (Figure 4A). The primitive mantle-normalized multi-element diagram (Figure 4A) shows both andesite and rhyolite samples share features similar to arc igneous rocks, such as enrichment of LILEs (e.g., Rb, U, K and Pb) and HFSEs (e.g., Nb, Ta, P and Ti) (Figure 4B). The variable negative Ba and Sr suggest that there was a relict of plagioclase and hornblende in the magma source or that these two minerals fractionated during an earlier magmatic stage. These characteristics are more remarkable in rhyolites on the primitive mantle-normalized diagram compared to the andesites in Hainan Island and volcanic rocks in the Andes Arc (Figure 4; the average geochemical data of volcanic rocks in the Andes Arc are based on the data from Tormey et al. (1995); Kay et al. (2005); Mamani et al., 2008; Mamani et al., 2009; Schiano et al. (2010); Folkes et al. (2011); Garrison et al. (2011); Pistolesi et al. (2015); Anderson et al. (2017); Bablon et al. (2020)).

5 Discussion

5.1 Magmatic evolution and source of the mid-Cretaceous volcanic rocks in southern Hainan Island

The FeO*, MgO, TiO_2, Al_2O_3, P_2O_5 and CaO contents of volcanics in southern Hainan Island decrease with increasing SiO_2 contents (Figure 5), but K_2O contents increase, similar to the relationships found in volcanic rocks from the Andes Arc (Tormey et al., 1995; Kay et al., 2005; Mamani et al., 2008; Mamani et al., 2009; Schiano et al., 2010; Folkes et al., 2011; Garrison et al., 2011; Pistolesi et al., 2015; Anderson et al., 2017; Bablon et al., 2020). The significant linear relationships between concentrations of the major elements in all samples of the study area imply that the magmatic sources of basic-intermediate-acid volcanic rocks are relatively consistent, and the volcanic magmas underwent similar magmatic evolution processes. The fractionation of dark minerals, plagioclases and apatites contributed to the decrease in most of major element contents, such as FeO*, CaO and P_2O_5. In addition, Zhou et al. (2015) determined that the $^{87}Sr/^{86}Sr(t)$ ratios of volcanics in the Liuluocun Formation range from 0.707532 to 0.7089651, and $\varepsilon_{Nd}(t)$ values range from −4.09 to −2.35. These narrow isotopic ranges indicate that the mid-Cretaceous magmatic sources in southern Hainan Island were relatively uniform and close to an EM-II type source.

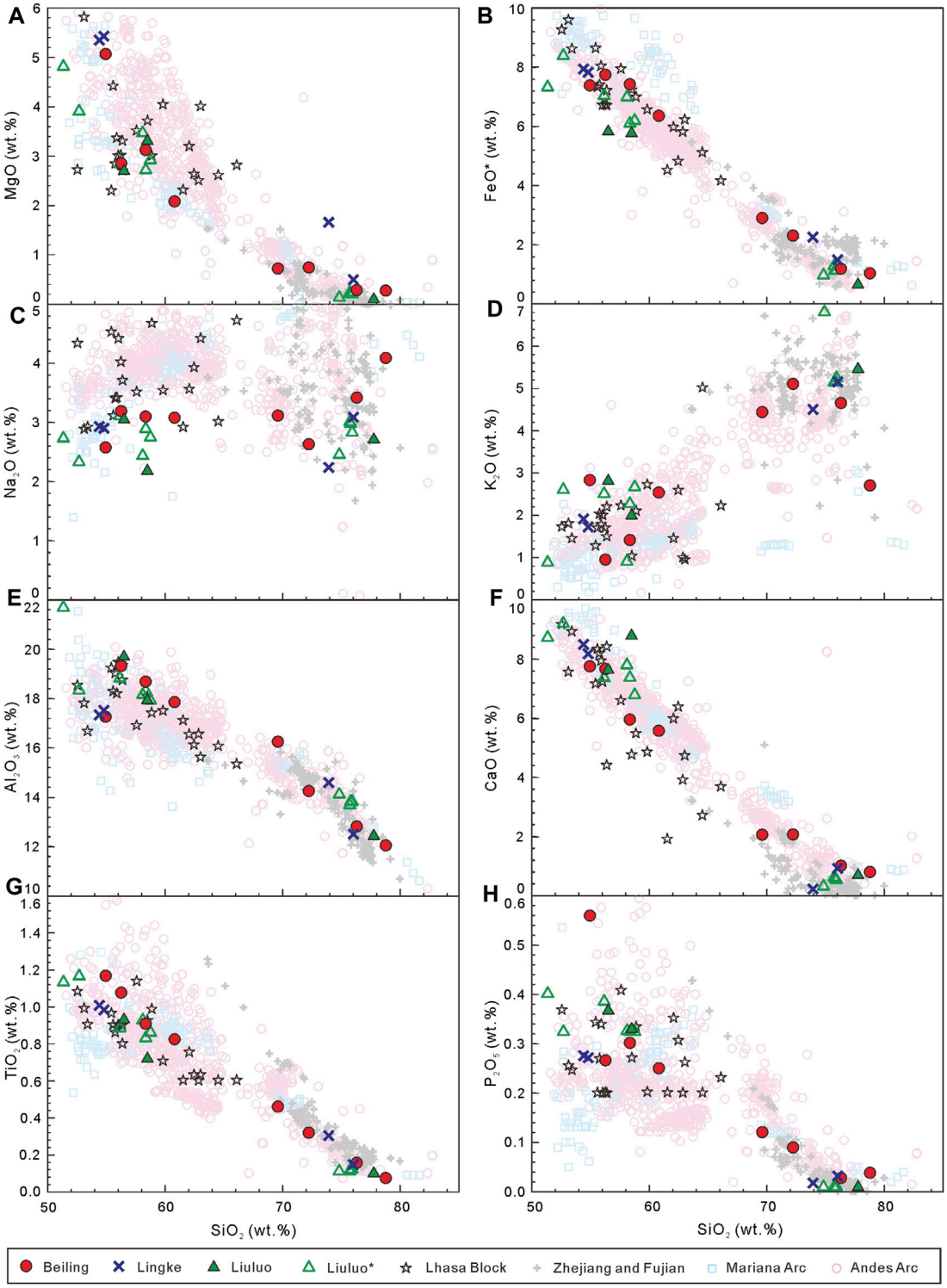

FIGURE 5
Selected major element oxides versus SiO_2 plots for Cretaceous volcanic rocks from southern Hainan Island. The geochemical data of volcanic rocks of Liuluo* are from Zhou et al. (2015a).

The high La/Yb and Th/La ratios of the volcanic rocks indicate an arc-type magmatic source during the mid-Cretaceous in southern Hainan Island (Figure 6A). The narrow ranges of La/Yb and U/Th ratios, combined with the significantly elevated Th/Ta and Th/Nb ratios (Figures 6A, B), suggest that the magmas originated from the EM-II type source with inputs of continental crust material, as in the Andes Arc. Liu et al. (2020, 2021) showed that the andesites in Guangdong and Guangxi, north of Hainan Island, also had similar

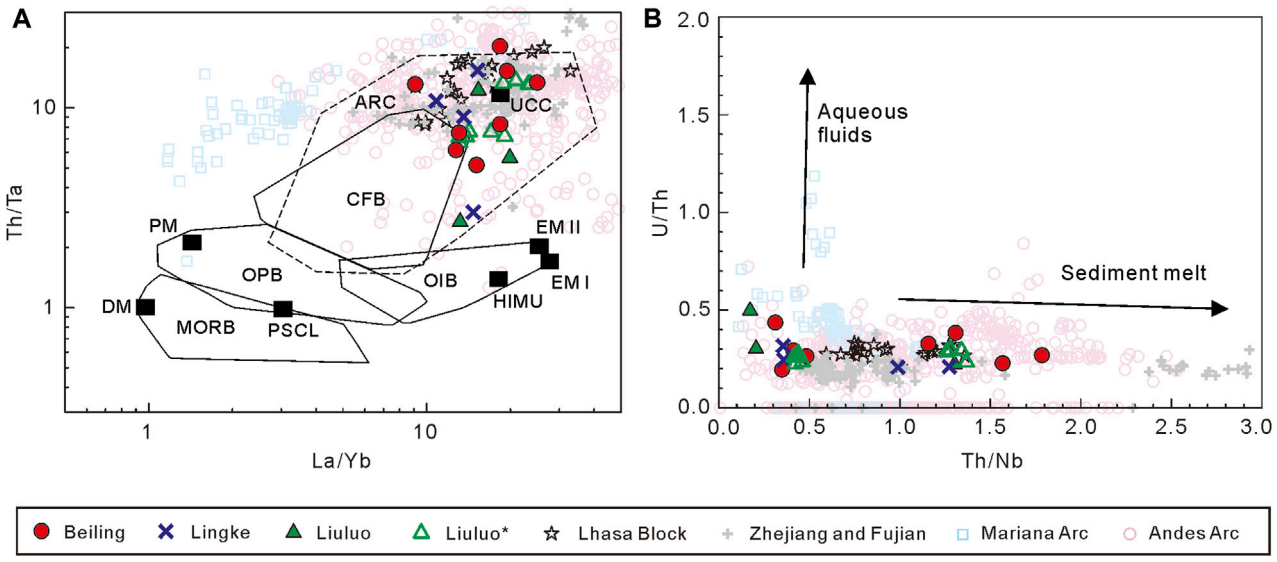

FIGURE 6
(A) Th/Ta vs. La/Yb diagram (after Ernst and Buchan, 2003) and **(B)** U/Th vs. Th/Nb diagram (after Kohut et al., 2006) for Cretaceous volcanic rocks from southern Hainan Island. Abbreviations: MORB, mid-ocean ridge basalt; OIB, ocean island basalt; CFB, continental flood basalt; OPB, oceanic plateau basalt; ARC, subduction zone basalt; Principle mantle reservoirs are: EM I (enriched mantle I), EM II (enriched mantle II), HIMU("High μ", μ= $^{238}U/^{204}Pb$), DMM (depleted MORB mantle) and FOZO (focal zone). Additional components are PM (primitive mantle), PSCL (post-Archean subcontinental lithosphere), and UCC (upper continental crust).

geochemical characteristics, and the mid-Cretaceous magmatic sources were altered by the melt of continental sediments. In addition, zircon $\varepsilon_{Hf}(t)$ data range from −9.73 to +0.47 (Zhou et al., 2015a), which is the result of the addition of continental crust materials to the magmatic source.

The input of continental materials into a magmatic source can occur during subduction. A large number of mid-Cretaceous andesites indicate that a subduction tectonic environment impacted Hainan Island during the Cretaceous. These andesites exhibit geochemical characteristics like Andean andesites, including remarkably high La/Yb ratios, high Th/Yb ratios and low Sc/Ni ratios (Figures 7A, B). These geochemical features also imply that the western margin of the SCS represented an Andes-type active continental margin during the Cretaceous period. Additionally, the presence of negative Eu anomalies, relatively flat chondrite normalized HREE patterns, low Y contents and low Sr/Y ratios observed in high-Mg andesites bear resemblance to sanukitic high-Mg andesites (Kamei et al., 2004; Tatsumi, 2006; Tang and Wang, 2010). These high-Mg andesites are believed to originate from the mantle peridotite that has undergone metasomatism by melts derived from subducted slab and sediments (Tatsumi, 2001; 2006). Moreover, the formation of these andesites can be attributed to ridge subduction tectonics (Tatsumi, 2001; 2006; Tang and Wang, 2010). At the same time, rhyolites in the study area have low (Zr + Nb +Ce + Y) values and FeO*/MgO ratios (Figure 7C), which are similar to I-type or S-type granites that mainly form under a compressional tectonic setting (Lu and Sang, 2004). The lower Y+Nb values and Rb contents of magmatic rocks also imply that the rhyolites were formed in the volcanic arc tectonic environment (Figure 7D; Pearce et al., 1984).

In summary, the geochemical characteristics of the andesites and rhyolites of southern Hainan Island indicate that the volcanic rocks were formed in a volcanic arc tectonic setting. The high but relatively similar Zr contents, combined with the low Ti contents which exhibited a wide range in values (Figure 8A), not only show that these volcanic magmas are of the arc type, but also indicate a magmatic evolution similar to those in Mexico, Ecuador, Chile and other regions (Pearce and Norry, 1979). Furthermore, Hainan Island experienced an active continental margin tectonic setting during the mid-Cretaceous that was an Andes-type active continental margin. Because of the fluids or melts in subduction zones, the Th/Yb ratio increases (Figure 8B), leading to enrichment of the geochemical characteristics due to subduction of volcanic rocks in the northwestern SCS during the mid-Cretaceous.

5.2 Tectonic setting of the western SCS margin during the mid-Cretaceous

The Cretaceous tectonics of Hainan Island and its surrounding areas are often regarded as the southwestern part of the magmatic belt in the eastern SCB, which resulted from the westward subduction of the paleo-Pacific Plate (Li et al., 1999; Thuy et al., 2004; Geng et al., 2006; Yan et al., 2010; Wang et al., 2012; Tang et al., 2014; Zhou et al., 2015a; Xu et al., 2016; Sun et al., 2017; Yan et al., 2017; Nong et al., 2021). However, many differences were found by analyzing the late Mesozoic magmatic activities on Hainan Island and the eastern SCB as detailed below.

First, the mid-Cretaceous (c.a. 100 Ma) volcanic rocks in the Zhejiang-Fujian area are characterized as rhyolite-dominated bimodal volcanic suits, with few records of andesite (Chen et al., 2008; Li et al., 2014; Liu et al., 2016). In contrast, intermediate acid volcanic rocks dominate in southern Hainan Island, and andesites have also been reported in southeastern Guangxi, western

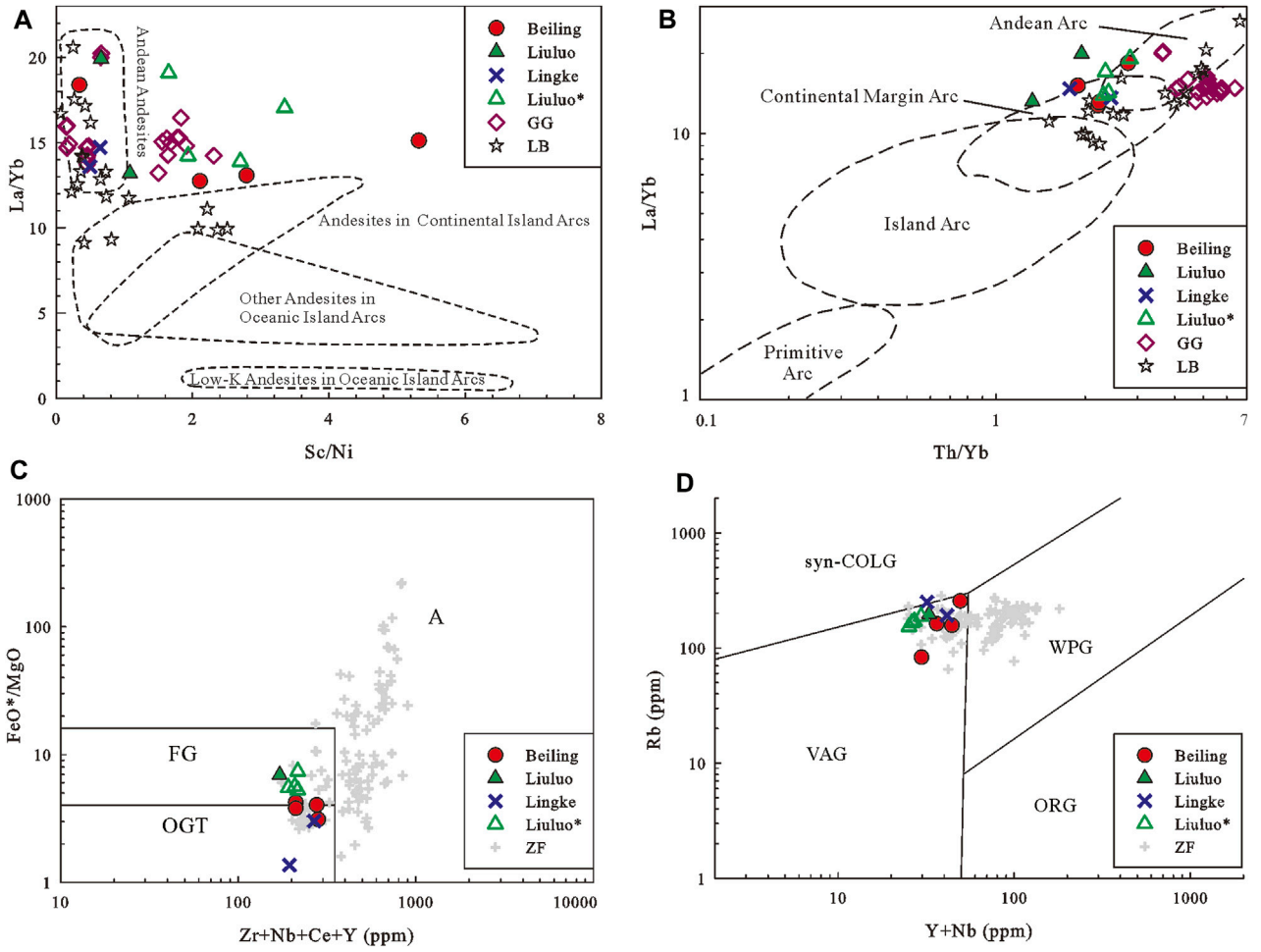

FIGURE 7
(A) La/Yb vs. Sc/Ni diagram (after Bailey, 1981) and **(B)** La/Yb vs. Th/Yb diagram (after Condie, 1986) for Cretaceous andesitic rocks from southern Hainan Island; **(C)** FeO*/MgO vs. (Zr+Nb+Ce+Y) diagram (after Whalen et al., 1987) and **(D)** Rb vs. (Y+Nb) diagram (after Pearce et al., 1984) for Cretaceous rhyolitic rocks from southern Hainan Island and its adjacent areas. Annotations: The geochemical data of mid-Cretaceous volcanic rocks in Guangxi and Guangdong are from Liu et al. (2021) and Jiang et al. (2015). The geochemical data of those in the Lhasa Block are from Ran et al. (2019) and Zhang et al. (2019a). The geochemical data of those in Zhejiang and Fujian are from Lapierre et al. (1997), Yu et al. (2008), Yan et al., 2016, Yan et al., 2018, Hong (2012), Hong et al. (2013), Li et al. (2017), and Qiu. et al. (1999a). Abbreviations: FG, fractionated felsic granites, OGT, unfractionated M-, I- and S-type granites; VAG, volcanic arc granites; syn-COLG, syn-collision granites; WPG, within plate granites; ORG, ocean ridge granites; GG, Guangxi and Guangdong; LB, Lhasa Block; ZF, Zhejiang and Fujian.

Guangdong and southern Vietnam, surrounding Hainan Island (Jiang et al., 2015; Liu et al., 2020; Liu et al., 2021). Besides, there are contemporaneous diorites reported in Hainan Island (Dilek and Tang, 2020). Intermediate magmatic activities were strong on the western margin of the SCS during the mid-Cretaceous. In addition, rhyolites in Hainan Island contain a small amount of K_2O and (Zr+Nb+Ce+Y) (Figure 3B; Figure 7C), showing volcanic arc settings (Figure 7D). While some mid-Cretaceous rhyolites in Zhejiang and Fujian are more alkaline and indicate extensional settings (Figures 3A, B; Figure 7D), namely, back-arc extensional environment (Yan et al., 2018; Guo et al., 2021).

Secondly, the rhyolites from Zhejiang and Fujian exhibit higher temperatures (determined using the method described in Watson and Harrison, 1983), such as those from Yandangshan (786°C–864°C, Yan et al., 2016) and Yunshan (861°C–930°C, Yan et al., 2018). The Paleo-Pacific plate subduction changed from a low-angle subduction during the Jurassic period to a high-angle subduction during the Cretaceous (Zhou and Li, 2000; Zhou et al., 2006). Rhyolites had high zircon-saturation temperatures in the mantle-upwelling tectonic setting due to the back-arc extension in Zhejiang and Fujian (Yan et al., 2016; Yan et al., 2018). However, saturation temperatures of acid volcanic rocks in southern Hainan Island are much lower, primarily ranging from 746°C–790°C with a temperature outside of this range (808°C) in only one sample. Thus, the magmatic activities in the southwestern SCB did not produce rocks with the characteristics of those experiencing lithospheric extension and high magmatic temperatures as the result of mantle upwelling, like in the eastern coastal area of the SCB.

Thirdly, from the central to the coastal areas of the SCB, the age of magmatic rocks gradually decreases, indicating the magmatic arc migrated south-eastward during the Yanshanian period (around the Jurassic-Cretaceous) (Zhou and Li, 2000; Zhou et al., 2006; Li et al., 2007; Liu et al., 2012; Zhou et al., 2015a). As a result, Cretaceous

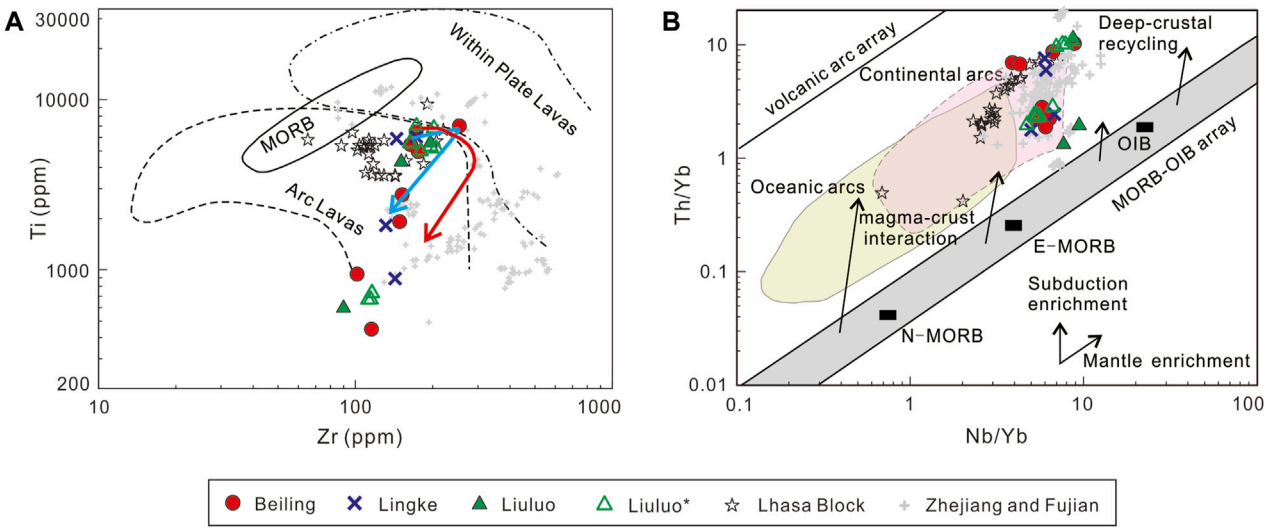

FIGURE 8
(A) Ti vs. Zr diagram (after Pearce and Norry, 1979; Pearce et al., 1981) and **(B)** Th/Yb vs. Nb/Yb diagram (after Pearce and Peate, 1995) for Cretaceous volcanic rocks from southern Hainan Island and its adjacent areas. Annotations: **(A)** the blue and red lines represent the Ti-depletion trends of magmatic rocks from Mexico-Ecuador and Chile, respectively, for amphibole and biotite fractionation. **(B)** The light green area represents oceanic arcs, and the pink area represents continental arcs. The legend for **(A, B)** is consistent with Figure 7. The geochemical data of mid-Cretaceous volcanic rocks from the Lhasa Block are from Ran et al. (2019) and Zhang et al. (2019a). The geochemical data representing Zhejiang and Fujian are from Lapierre et al. (1997), Qiu et al. (1999a), Yu et al. (2008), Hong (2012), Hong et al. (2013), Yan et al. (2016), Yan et al. (2018), Li et al. (2017), Guo et al. (2012), and Guo et al. (2021).

magmatic activity was concentrated in the eastern coastal area of Zhejiang and Fujian (Zhou and Li, 2000; Zhou et al., 2006). According to the retreat model of paleo-Pacific subduction (Zhou and Li, 2000; Zhou et al., 2006), the magmatic activity of Hainan Island in the mid-Cretaceous should be significantly weaker than during the Jurassic, due to its southwestern location in the SCB. However, the Jurassic strata in Hainan Island are not developed, and there were no Jurassic volcanic rock records. The exposed area of Jurassic granitoids is about 572.2 km^2, while the Cretaceous granitoids, mainly concentrated around the ages of 110–90 Ma, have an exposed area of more than 2900 km^2 (Hainan Geological Survey, 2004; Yichang IGMR and Hainan GS, 2004; Hainan Geological Survey, 2007). Therefore, the magmatic activities in the mid-Cretaceous were much stronger than during the Jurassic.

Finally, mid-Cretaceous alkaline granites, containing alkaline dark minerals, have been found in coastal areas of Zhejiang and Fujian (Qiu et al., 1996; Qiu et al., 1999b; Qiu et al., 2000; Xiao et al., 2007; Zhao et al., 2018) (Figure 1B), and have very high Ga/Al values and (Zr + Ce + Nb + Y) contents. They are typical A-type granites and provide powerful evidence of an extensional environment in the eastern part of the SCB, which resulted from the rollback of the paleo-Pacific Plate or the oblique subduction (Zhou and Li, 2000; Zhou et al., 2006; Li et al., 2007; Li and Li, 2007; Wong et al., 2009). In contrast, on Hainan Island and its adjacent areas on the western margin of the SCS, I- and S-type granitoids are reported widely, without reports of typical A-type granitoids from the mid-Cretaceous.

In summary, the western margin of the SCS, where Hainan Island is located, was not influenced by the paleo-Pacific subduction, which controlled the tectonic and magmatic evolution of the eastern SCB in areas such as Zhejiang and Fujian. Previous work has shown that the subduction of the paleo-Pacific to East Asia in the Cretaceous mainly affected the area east of Wuyi Mountain (Figure 1B; Chen et al., 2005; Zhang et al., 2017). Previous studies (Yan et al., 2014; Hennig et al., 2017; Ye et al., 2018; Guo et al., 2021) have reported that contemporaneous magmatic records in the eastern and southern microblocks around Hainan Island, emphasizing the more western interior of Hainan Island that was unlikely to be within the subduction range of the paleo-Pacific plate. At that time, the paleo-Pacific subduction could not have contributed to the arc-type magmatic activities on Hainan Island and its adjacent areas, and the western margin of the SCS was not within the affected range of the paleo-Pacific subduction. In the view of the fact that the southeastern edge of the Eurasian plate, where Hainan Island is located, is adjacent to the Tethys tectonic belts to the west, more attention should be paid to the impact of the Tethys on the western SCS.

At ca. 100 Ma, the Neotethyan ridge subducted northward, and upwelling of the hot asthenosphere along the slab window caused the partial melting of the subducted oceanic slab and mantle wedge, resulting in strong magmatism (Zhang et al., 2019a; Zhang et al., 2019b). As a result, adakitic rocks and the high-Mg andesites of this period were exposed in southeastern Lhasa Terrane (Zhang et al., 2019a; Zhang et al., 2019b). At similar times on Hainan Island, the granitoids from Qianjia and Tunchang also show the geochemical characteristics of adakites, such as high Sr/Y ratios with low Y and Yb contents (Wang et al., 2012; Sun et al., 2018). Kelemen (1995) limited the $Mg^{\#}$ value of high-Mg andesite to 45, which means that some andesites of the Liuluocun and Lingkecun Formations are high-Mg andesite. There were high-Mg andesites-adakitic rocks in the mid-Cretaceous assemblage on Hainan Island. This mid-Cretaceous assemblage is also found in Guangxi and Guangdong, to the north of Hainan Island (Sun et al., 2017; Zhang et al., 2017; Liu et al., 2020; Liu et al., 2021). In the modern subduction zones, this

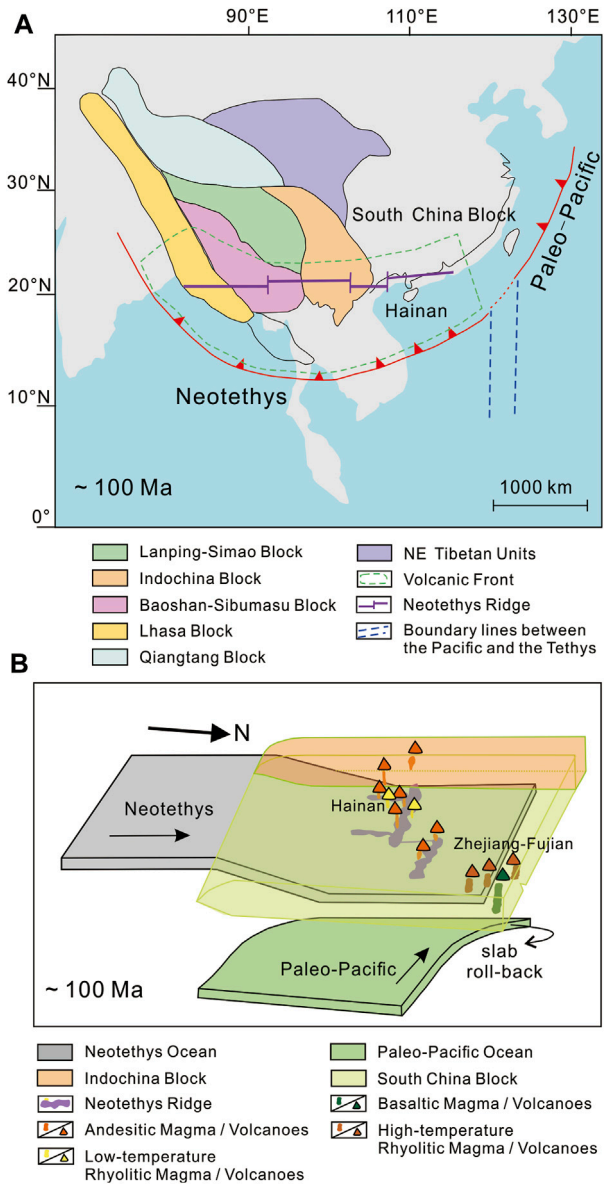

FIGURE 9
Sketched maps of **(A)** tectonic plate reconstruction at ~100 Ma and **(B)** magmatic activities in the study area at ~100 Ma (based on Royden et al., 2008; Zhang et al., 2017; Zhang et al., 2023). Annotations: **(A)** Grey areas show the present location of blocks. Red lines are estimated positions of subduction zones. Blue lines show the boundary lines between the paleo-Pacific and the Tethys. **(B)** The magma in Zhejiang and Fujian is shown in dark red to show its higher temperature compared to that in Hainan Island The paleo-Pacific oceanic plate subducted northwestward (Li et al., 2020), while the Neothethys subducted northward (Zhang et al., 2023).

type of assemblage is often related to the subduction of the ocean ridge (Sajona et al., 2000; Bourdon et al., 2003; Castillo, 2008). The same assemblage occurs both in the western margin of the SCS and the eastern Lhasa Terrane and is the same age, which indicates that the two areas were in the special tectonic setting of the subducting Neotethyan ridge (Figure 9). Moreover, the basalts in southern Hainan Island exhibit Nb contents ranging from 9.20–10.79 ppm (Zhou et al., 2015a), while the Nanxiong basalts (96 Ma) in Guangdong Province, north of Hainan Island display Nb contents between 22.61-24.28 ppm (Shu et al., 2004), indicating their enriched-Nb characteristics. Additionally, the Cretaceous mafic dikes (101–93 Ma) on Hainan Island contains Nb concentrations of 12.36–20.22 ppm (Tang et al., 2010), further supporting the exitence of Nb-enriched basaltic magma in this region and its surrounding during this time as well as ridge subduction processes (Wang et al., 2020). During the mid-Cretaceous period, Neotethyan ridge began to subduct northward into southern Asia. Consequently, young oceanic slab and terrigenous sediments melted upon subduction and metasomatized the mantle wedge (Tatsumi, 2001; Tatsumi, 2006). As a result of these geological processes occurring simultaneously across different regions within Southeastern Lhasa Terrane and Hainan Island high-Mg andesites-adakitic rocks were formed.

Due to the opening of the SCS and subsequent extrusion tectonic movement in Asia (Tapponnier et al., 1982), Hainan Island is geographically distant from the Neotethys suture zone located southwest of Sumatra Island and Borneo Island (Zahirovic et al., 2016). According to a paleomagnetic study of the Khorat Basin on the Indochina Block, the collision between India and Asia caused the Khorat Basin to move 950 ± 150 km southward and rotate clockwise by 16°–17° relative to the SCB (Charusiri et al., 2006). Another study by Singsoupho et al. (2014) suggests the southern transport was 750–1700 km. Thus, the paleolatitude of the southern margin of the Indochina Block and the northern margin of the SCS were roughly the same in the late Mesozoic, leading to the formation of a nearly E-W trending magmatic belt from Hainan Island to the Lhasa Block. Cretaceous granitoids are found in many places in the south of this belt, such as the Xisha Islands, Mekong Basin, South Con Son Basin, Natuna Islands, Malay Peninsula, and Singapore (Areshev et al., 1992; Li et al., 1999; Yan et al., 2010; Yan et al., 2014; Oliver et al., 2011; Ng et al., 2015; Zhu et al., 2017; Gillespie et al., 2019), which also resulted from the northward subduction of the Neotethys. Considering different generations of the Tethys Ocean may be characterized as land (islands) alternating with seas (just as Indonesian Archipelago; Fang, 2002), the possibility cannot be ruled out that the area of sea affecting the northwestern part of the SCS was a branch of the Neotethys. This does not conflict with the tectonic framework of the western margin of SCS, which was affected by the subduction structure of the Neotethys in the Cretaceous.

6 Conclusion

(1) The volcanic rocks of southern Hainan Island are an assemblage of basaltic andesite-andesite-rhyolite, belonging to high-K calc-alkaline series or calc-alkaline series, with metaluminous-peraluminous characteristics. The andesites and rhyolites are enriched in LREEs with positively skewed REE distribution curves, and negative Eu anomalies of the rhyolites are obvious. Additionally, they are enriched in LILEs and depleted in HFSEs.

(2) There are a large number of mid-Cretaceous andesites on Hainan Island, and acid volcanic rocks formed at low temperatures. No A-type granite of the same age was found, indicating the tectonics of Hainan Island were not influenced by the subduction of the paleo-Pacific Plate in the mid-Cretaceous.

(3) The geochemical characteristics of the mid-Cretaceous andesites and rhyolites indicate an active continental margin tectonic setting on Hainan Island. The high-Mg andesites and adakitic rocks of Hainan Island and its adjacent area can also be found in the Lhasa Block. During the mid-Cretaceous, the western margin of the SCS was mainly affected by the subduction of the Neotethys.

Data availability statement

The original contributions presented in the study are included in the article/Supplementary material, further inquiries can be directed to the corresponding author.

Author contributions

YL, NF, and ZW designed the research. YL and NF conducted fieldwork, collecting samples. YL, NF, and ZW conducted the lab work. YL and ZW wrote the paper. NF revised the paper critically for important intellectual content. All authors contributed to the article and approved the submitted version.

Funding

This research was supported by the National Natural Science Foundation of China (Nos 41876059, 41572207, 41276047, 41030853), Shantou University Scientific Research Initiation Grant (No. NTF20028), China Geological Survey (No. DD20208013), and China-ASEAN Maritime Cooperation Fund (121201005000151110).

Acknowledgments

The authors acknowledge Dr. Zhou Yingchun from the Institute of Hainan Geological Bureau and Dr. Lu Shihui from China University of China, Beijing, for their support during the field investigation. The authors thank Prof. Zhao Hailing from the China University of Geosciences, Beijing, for her helpful discussions.

Conflict of interest

The authors declare that the research was conducted in the absence of any commercial or financial relationships that could be construed as a potential conflict of interest.

Publisher's note

References

Andersen, N. L., Singer, B. S., Jicha, B. R., Beard, B. L., Johnson, C. M., and Licciardi, J. M. (2017). Pleistocene to Holocene Growth of a Large Upper Crustal Rhyolitic Magma Reservoir beneath the Active Laguna del Maule Volcanic Field, Central Chile. *J. Petrol.* 58 (1), 85–114. doi:10.1093/petrology/egx006

Areshev, E. G., Dong, T. L., San, N. T., and Shnip, O. A. (1992). Reservoirs in fractured basement on the continental shelf of Southern Vietnam. *J. Pet. Geol.* 15 (4), 451–464. doi:10.1111/j.1747-5457.1992.tb01045.x

Bablon, M., Quidelleur, X., Siani, G., Samaniego, P., Le Pennec, J. L., Nouet, J., et al. (2020). Glass shard K-Ar dating of the chalupas caldera major eruption: main pleistocene stratigraphic marker of the Ecuadorian volcanic arc. *Quat. Geochronol.* 57 (9), 101053. doi:10.1016/j.quageo.2020.101053

Bailey, J. C. (1981). Geochemical criteria for a refined tectonic discrimination of orogenic andesites. *Chem. Geol.* 32 (1), 139–154. doi:10.1016/0009-2541(81)90135-2

Bloomer, S. H., Stern, R. J., Fisk, E., and Geschwind, C. H. (1989). Shoshonitic volcanism in the northern Mariana Arc: 1. Mineralogic and major and trace element characteristics. *J. Geophys. Res.-Solid Earth* 94 (B4), 4469–4496. doi:10.1029/JB094iB04p04469

Bourdon, E., Eissen, J. P., Gutscher, M. A., Monzier, M., Hall, M. L., and Cotton, J. (2003). Magmatic response to early aseismic ridge subduction: the Ecuadorian margin case (south America). *Earth Planet. Sci. Lett.* 205 (3–4), 123–138. doi:10.1016/S0012-821X(02)01024-5

Cai, D., and Fu, G. (1997). Classification and correlation of Tong'anling-Niulaling volcanic strata in southern Hainan. *Regional Geol. China* 16 (4), 348–358.

Castillo, P. R. (2008). Origin of the adakite-high-Nb basalt association and its implications for postsubduction magmatism in Baja California, Mexico. *Geol. Soc. Am. Bull.* 120 (3-4), 451–462. doi:10.1130/B26166.1

Charusiri, P., Imsamut, S., Zhuang, Z., Ampaiwan, T., and Xu, X. (2006). Paleomagnetism of the earliest cretaceous to early late cretaceous sandstones, Khorat Group, northeast Thailand: implications for tectonic plate movement of the Indochina block. *Gondwana Res.* 9, 310–325. doi:10.1016/j.gr.2005.11.006

Chen, C. H., Lee, C. Y., Lu, H. Y., and Hsieh, P. S. (2008). Generation of late cretaceous silicic rocks in SE China: age, major element and numerical simulation constraints. *J. Asian Earth Sci.* 31 (4-6), 479–498. doi:10.1016/j.jseaes.2007.08.002

Chen, W. F., Chen, P. R., Xu, X. S., and Zhang, M. (2005). Geochemical characteristics of Cretaceous basaltic rocks in South China and constraints on Pacific plate subduction. *Sci. China Ser. D-Earth Sci.* 48 (12), 2104–2117. doi:10.1360/04yd0149

Condie, K. C. (1986). Geochemistry and tectonic setting of early proterozoic supracrustal rocks in the southwestern United States. *J. Geol.* 94 (6), 845–864. doi:10.1086/629091

Dilek, Y., and Tang, L. (2020). Magmatic record of the mesozoic geology of hainan island and its implications for the mesozoic tectonomagmatic evolution of SE China: effects of slab geometry and dynamics in continental tectonics. *Geol. Mag.* 158, 118–142. doi:10.1017/S0016756820001211

Dixon, T. H., and Batiza, R. (1979). Petrology and chemistry of recent lavas in the northern marianas: implications for the origin of island arc basalts. *Contrib. Mineral. Petrol.* 70 (2), 167–181. doi:10.1007/bf00374446

Elliott, T., Plank, T., Zindler, A., White, W., and Bourdon, B. (1997). Element transport from slab to volcanic front at the Mariana arc. *J. Geophys. Res.-Solid Earth* 102 (B7), 14991–15019. doi:10.1029/97jb00788

Ernst, R. E., and Buchan, K. L. (2003). Recognizing mantle plumes in the geological record. *Annu. Rev. Earth Planet. Sci.* 31, 469–523. doi:10.1146/annurev.earth.31.100901.145500

Fang, N. (2016). A new model on the mesozoic "south China sea" (SCS): reconstructing the hainan marginal Arc and recognizing the tethyan SCS. *Earth Sci. Front.* 23 (6), 107–119. doi:10.13745/j.esf.2016.06.008

Fang, N. Q. (2002). Major Features of the sedimentary records from the Indonesian archipelago and research on the Paleo-Tethys in Yunnan. *Earth Sci. Front.* 9 (3), 173–181.

Folkes, C. B., de Silva, S. L., Wright, H. M., and Cas, R. A. F. (2011). Geochemical homogeneity of a long-lived, large silicic system; evidence from the Cerro Galán caldera, NW Argentina. *Bull. Volcanol.* 73 (10), 1455–1486. doi:10.1007/s00445-011-0511-y

Garrison, J. M., Davidson, J. P., Hall, M., and Mothes, P. (2011). Geochemistry and Petrology of the most recent deposits from cotopaxi volcano, northern volcanic zone, Ecuador. *J. Petrol.* 52 (9), 1641–1678. doi:10.1093/petrology/egr023

Geng, H., Xu, X., O'Reilly, S. Y., Zhao, M., and Sun, T. (2006). Cretaceous volcanic-intrusive magmatism in western Guangdong and its geological significance. *Sci. China Ser. D-Earth Sci.* 49 (7), 696–713. doi:10.1007/s11430-006-0696-7

Gillespie, M. R., Kendall, R. S., Leslie, A. G., Millar, I. L., Dodd, T. J. H., Kearsey, T. I., et al. (2019). The igneous rocks of Singapore: new insights to Palaeozoic and Mesozoic assembly of the Sukhothai Arc. *J. Asian Earth Sci.* 183, 103940. doi:10.1016/j.jseaes.2019.103940

Guangdong BGMR (1988). *Regional Geology of Guangdong Province*. Beijing: Geological Publishing House, 1–602.

Guo, F., Fan, W., Li, C., Zhao, L., Li, H., and Yang, J. (2012). Multi-stage crust-mantle interaction in SE China: temporal, thermal and compositional constraints from the mesozoic felsic volcanic rocks in eastern guangdong-fujian provinces. *Lithos* 150, 62–84. doi:10.1016/j.lithos.2011.12.009

Guo, F., Wu, Y., Zhang, B., Zhang, X., Zhao, L., and Liao, J. (2021). Magmatic responses to cretaceous subduction and tearing of the paleo-Pacific Plate in SE China: an overview. *Earth-Sci. Rev.* 212, 103448. doi:10.1016/j.earscirev.2020.103448

Hainan Geological Survey (2007). *Regional geological survey report of 1: 250000 dongfang county sheet in hainan Province*. Haikou: Hainan GS, 120–200.

Hainan Geological Survey (2004). *Regional geological survey report of 1: 250000 qionghai county sheet in hainan Province*. Haikou: Hainan GS, 19–34.

Hennig, J., Breitfeld, H. T., Hall, R., and Nugraha, A. S. (2017). The Mesozoic tectono-magmatic evolution at the Paleo-Pacific subduction zone in West Borneo. *Gondwana Res.* 48, 292–310. doi:10.1016/j.gr.2017.05.001

Hole, M. J., Saunders, A. D., Marriner, G. F., and Tarney, J. (1984). Subduction of pelagic sediments: implications for the origin of Ce-anomalous basalts from the Mariana islands. *J. Geol. Soc.* 141 (3), 453–472. doi:10.1144/gsjgs.141.3.0453

Hong, W. T. (2012). *Geochronological, geochemical and petrogenetic studies of the Yunshan bimodal volcanic rocks, SE China*. Nanjing China: Nanjing University, 1–44.

Hong, W. T., Xu, X. S., and Zou, H. B. (2013). Petrogenesis of coexisting high-silica aluminous and peralkaline rhyolites from Yunshan (Yongtai), southeastern China. *J. Asian Earth Sci.* 74, 316–329. doi:10.1016/j.jseaes.2013.01.005

Huang, W., Liang, H., Zhang, J., Wu, J., Chen, X., and Ren, L. (2019). Genesis of the Dachang Sn-polymetallic and Baoshan Cu ore deposits, and formation of a Cretaceous Sn-Cu ore belt from southwest China to western Myanmar. *Ore Geol. Rev.* 112, 103030. doi:10.1016/j.oregeorev.2019.103030

Irvine, T. N., and Baragar, W. R. A. (1971). A guide to the chemical classification of the common volcanic Rocks. *Can. J. Earth Sci.* 8 (5), 523–548. doi:10.1139/e71-055

Jiang, Y., Liang, X., Liang, X., Zhou, Y., Wen, S., Fu, J., et al. (2015). Geochronology, geochemistry and petrogenesis of Cretaceous andesitic porphyrite from Renhua area, northern Guangdong, SE China. *Geotect. Metallogenia* 39 (3), 481–496. doi:10.16539/j.ddgzyckx.2015.03.010

Kamei, A., Owada, M., Nagao, T., and Shiraki, K. (2004). High-Mg diorites derived from sanukitic HMA magmas, kyushu island, southwest Japan arc: evidence from clinopyroxene and whole rock compositions. *Lithos* 75 (3-4), 359–371. doi:10.1016/j.lithos.2004.03.006

Kay, S. M., Godoy, E., and Kurtz, A. (2005). Episodic arc migration, crustal thickening, subduction erosion, and magmatism in the south-central Andes. *Geol. Soc. Am. Bull.* 117 (1), 67–88. doi:10.1130/B25431.1

Kelemen, P. B. (1995). Genesis of High Mg# andesites and the continental crust. *Contrib. Mineral. Petrol.* 120, 1–19. doi:10.1007/bf00311004

Klaver, M., Lewis, J., Parkinson, I. J., Elburg, M. A., Vroon, P. Z., Kelley, K. A., et al. (2020). Sr isotopes in arcs revisited: tracking slab dehydration using $\delta^{88/86}$Sr and ^{87}Sr/^{86}Sr systematics of arc lavas. *Geochim. Cosmochim. Acta* 288, 101–119. doi:10.1016/j.gca.2020.08.010

Kohut, E. J., Stern, R. J., Kent, A. J. R., Nielsen, R. L., Bloomer, S. H., and Leybourne, M. (2006). Evidence for adiabatic decompression melting in the Southern Mariana Arc from high-Mg lavas and melt inclusions. *Contrib. Mineral. Petrol.* 152 (2), 201–221. doi:10.1007/s00410-006-0102-7

Lapierre, H., Jahn, B. M., Charvet, J., and Yu, Y. W. (1997). Mesozoic felsic arc magmatism and continental olivine tholeiites in Zhejiang province and their relationship with the tectonic activity in southeastern China. *Tectonophysics* 274, 321–338. doi:10.1016/s0040-1951(97)00009-7

Le Bas, M. J., Le Maitre, R. W., Streckeisen, A., and Zanettin, B. (1986). A chemical classification of volcanic rocks based on the total alkali-silica diagram. *J. Petrol.* 27 (3), 745–750. doi:10.1093/petrology/27.3.745

Li, J., Cawood, P. A., Ratschbacher, L., Zhang, Y., Dong, S., Xin, Y., et al. (2020). Building Southeast China in the late mesozoic: insights from alternating episodes of shortening and extension along the lianhuashan fault zone. *Earth-Sci. Rev.* 201, 103056. doi:10.1016/j.earscirev.2019.103056

Li, P., Liang, H., Dai, Y., and Lin, H. (1999). Pulse compression for finite amplitude distortion based harmonic imaging using coded waveforms. *Geol. Guangdong* 14 (1), 1–16. doi:10.1177/016173469902100101

Li, X. H., Li, Z. X., Li, W. X., Liu, Y., Yuan, C., Wei, G., et al. (2007). U-Pb zircon, geochemical and Sr-Nd-Hf isotopic constraints on age and origin of jurassic I- and A-type granites from central Guangdong, se China: A major igneous event in response to foundering of a subducted flat-slab? *Lithos* 96, 186–204. doi:10.1016/j.lithos.2006.09.018

Li, X. Y., Li, S. Z., Suo, Y. H., Dai, L. M., Gu, L. L., Ge, F. J., et al. (2017). Late cretaceous basalts and rhyolites from shimaoshan Group in eastern fujian province, SE China: age, petrogenesis, and tectonic implications. *Int. Geol. Rev.* 60 (11-14), 1721–1743. doi:10.1080/00206814.2017.1353447

Li, Y., Dong, S., Zhang, Y., Li, J., Su, J., and Han, B. (2016). Episodic mesozoic constructional events of central south China: constraints from lines of evidence of superimposed folds, fault kinematic analysis, and magma geochronology. *Int. Geol. Rev.* 58 (9), 1076–1107. doi:10.1080/00206814.2016.1146999

Li, Z., Qiu, J. S., and Yang, X. M. (2014). A review of the geochronology and geochemistry of late yanshanian (cretaceous) plutons along the fujian coastal area of southeastern China: implications for magma evolution related to slab break-off and rollback in the cretaceous. *Earth-Sci. Rev.* 128, 232–248. doi:10.1016/j.earscirev.2013.09.007

Li, Z. X., and Li, X. H. (2007). Formation of the 1300-km-wide intracontinental orogen and postorogenic magmatic province in mesozoic south China: A flat-slab subduction model. *Geology* 35 (2), 179–182. doi:10.1130/G23193A.1

Li, Z. X., Li, X. H., Li, W. X., and Ding, S. (2008). Was cathaysia part of proterozoic laurentia? New data from hainan island, south China. *Terr. Nova* 20 (2), 154–164. doi:10.1111/j.1365-3121.2008.00802.x

Lin, P. N., Stern, R. J., and Bloomer, S. H. (1989). Shoshonitic volcanism in the northern Mariana Arc: 2. Large-Ion lithophile and rare earth element abundances: evidence for the source of incompatible element enrichments in intraoceanic arcs. *J. Geophys. Res.-Solid Earth* 94 (B4), 4497–4514. doi:10.1029/JB094iB04p04497

Liu, L., Xu, X., and Xia, Y. (2016). Asynchronizing paleo-pacific slab rollback beneath SE China: insights from the episodic late mesozoic volcanism. *Gondwana Res.* 37, 397–407. doi:10.1016/j.gr.2015.09.009

Liu, L., Xu, X., and Zou, H. (2012). Episodic eruptions of the late mesozoic volcanic sequences in southeastern Zhejiang, SE China: petrogenesis and implications for the geodynamics of paleo-pacific subduction. *Lithos* 154, 166–180. doi:10.1016/j.lithos.2012.07.002

Liu, Y., Fang, N., Qiang, M., Jia, L., and Song, C. J. (2021). Cox regression analysis for distorted covariates with an unknown distortion function. *Geoscience* 35 (4), 968–983. doi:10.1002/bimj.202000209

Liu, Y., Fang, N., Qiang, M., Jia, L., and Song, C. J. (2020). The Cretaceous igneous rocks in southeastern Guangxi and their implication for tectonic environment in southwestern South China Block. *Open Geosci.* 12 (1), 518–531. doi:10.1515/geo-2020-0160

Lu, F., and Sang, L. (2004). *Petrology: Granitoid rocks and related rocks*. Beijing: Geological Press, 82–95.

Mamani, M., Tassara, A., and Wörner, G. (2008). Composition and structural control of crustal domains in the central Andes. *Geochem. Geophys. Geosyst.* 9 (3), 1–13. doi:10.1029/2007GC001925

Mamani, M., Worner, G., and Sempere, T. (2009). Geochemical variations in igneous rocks of the central andean orocline (13°S to 18°S): tracing crustal thickening and magma generation through time and space. *Geol. Soc. Am. Bull.* 122 (1–2), 162–182. doi:10.1130/B26538.1

Maniar, P. D., and Piccoli, P. M. (1989). Tectonic discrimination of granitoids. *Geol. Soc. Am. Bull.* 101 (5), 635–643. doi:10.1130/0016-7606(1989)101<0635:TDOG>2.3.CO;2

Marske, J. P., Pietruszka, A. J., Trusdell, F. A., and Garcia, M. O. (2010). Geochemistry of southern pagan island lavas, Mariana Arc: the role of subduction zone processes. *Contrib. Mineral. Petrol.* 162 (2), 231–252. doi:10.1007/s00410-010-0592-1

National Standard of P.R. China GB/T14506.30-2010 (2011). *Determination of 44 elements*.

National Standard of P.R. China (2011a). *Determination of FeO content*.

National Standard of P.R. China (2011b). *Determination of 16 major and minor elements content*.

Ng, S. W. P., Whitehouse, M. J., Searle, M. P., Robb, L. J., Ghani, A. A., Chung, S. L., et al. (2015). Petrogenesis of Malaysian granitoids in the southeast asian tin belt: part 2. U-Pb zircon geochronology and tectonic model. *Geol. Soc. Am. Bull.* 127 (9–10), 1238–1258. doi:10.1130/B31214.1

Nong, A. T. Q., Hauzenberger, C. A., Gallhofer, D., and Dinh, S. Q. (2021). Geochemistry and zircon U-Pb geochronology of late mesozoic igneous rocks from SW vietnam-SE Cambodia: implications for episodic magmatism in the context of the paleo-pacific subduction. *Lithos* 390–391, 106101. doi:10.1016/j.lithos.2021.106101

Oliver, G. J. H., Khin, Z., Hotson, M. D., and Hammer, S. (2011). Accounting graduates and the capabilities that count: perceptions of graduates, employers and Accounting academics in four Australian universities. *Innov. Mag.* 10 (2), 2–27. doi:10.21153/jtlge2011vol2no1art550

Pistolesi, M., Cioni, R., Bonadonna, C., Elissondo, M., Baumann, V., Bertagnini, A., et al. (2015). Complex dynamics of small-moderate volcanic events: the example of the

2011 rhyolitic cordón caulle eruption, Chile. *Bull. Volcanol.* 77, 3. doi:10.1007/s00445-014-0898-3

Pearce, J. A., Alabaster, T., Shelton, A. W., and Searle, M. P. (1981). The Oman ophiolite as a cretaceous arc-basin complex: evidence and implications. *Philos. Trans. R. Soc. Lond.* 300, 299–317. doi:10.2307/36753

Pearce, J. A., Harris, N. B. W., and Tindle, A. G. (1984). Trace element discrimination diagrams for the tectonic interpretation of granitic rocks. *J. Petrol.* 25 (4), 956–983. doi:10.1093/petrology/25.4.956

Pearce, J. A., and Norry, M. J. (1979). Petrogenetic implications of Ti, Zr, Y, and Nb variations in volcanic rocks. *Contrib. Mineral. Petrol.* 69, 33–47. doi:10.1007/bf00375192

Pearce, J. A., and Peate, D. W. (1995). Tectonic implications of the composition of volcanic arc magmas. *Annu. Rev. Earth Planet. Sci.* 23, 251–285. doi:10.1146/annurev.ea.23.050195.001343

Peccerillo, A., and Taylor, S. R. (1976). Geochemistry of Eocene calc-alkaline volcanic rocks from the Kastamonu area, northern Turkey. *Contrib. Mineral. Petrol.* 58 (1), 63–81. doi:10.1007/bf00384745

Qiu, J., Kanisawa, S., and Wang, D. (2000). Geochemical characteristics and genetic type of yaokeng alkali granites in cangnan county, Zhejiang province. *Acta Petrologica Mineralogica* 19 (2), 97–105.

Qiu, J. S., Wang, D. Z., and Zhou, J. C. (1999a). Geochemistry and petrogenesis of the late Mesozoic bimodal volcanic rocks at Yunshan caldera, Yongtai county, Fujian province. *Acta Petrologica Mineralogica* 18 (2), 97–107.

Qiu, J., Wang, D., and Brent, I. A. M. (1999b). Geochemistry and petrogenesis of the I- and A-type composite granite masses in the coastal area of Zhejiang and Fujian province. *Acta Petrol. Sin.* 15 (2), 237–246.

Qiu, J., Wang, D., and Peng, Y. (1996). Petrology, geochemistry and genesis of Taohuadao alkali granite in Zhoushan, Zhejiang province. *J. Nanjiang Univ.* 32 (1), 80–89.

Ran, M. L., Kang, Z. Q., Xu, J. F., Yang, F., Jiang, Z. Q., Li, Q., et al. (2019). Evolution of the northward subduction of the neo-tethys:implications of geochemistry of cretaceous arc volcanics in qinghai-Tibetan plateau. *Paleogeogr. Paleoclimatol. Paleoecol.* 515, 83–94. doi:10.1016/j.palaeo.2017.12.043

Reagan, M. K., Hanan, B. B., Heizler, M. T., Hartman, B. S., and Hickey-Vargas, R. (2008). Petrogenesis of volcanic rocks from saipan and rota, Mariana islands, and implications for the evolution of nascent island arcs. *J. Petrol.* 49 (3), 441–464. doi:10.1093/petrology/egm087

Royden, L. H., Burchfiel, B. C., and van der Hilst, R. D. (2008). The geological evolution of the Tibetan Plateau. *Science* 321, 1054–1058. doi:10.1126/science.1155371

Sajona, F. G., Maury, R. C., Pubellier, M., Leterrier, J., Bellon, H., and Cotton, J. (2000). Magmatic source enrichment by slab-derived melts in a young post-collision setting, central Mindanao (Philippines). *Lithos* 54, 173–206. doi:10.1016/s0024-4937(00)00019-0

Schiano, P., Monzier, M., Eissen, J. P., Martin, H., and Koga, K. T. (2010). Simple mixing as the major control of the evolution of volcanic suites in the Ecuadorian Andes. *Contrib. Mineral. Petrol.* 160 (2), 297–312. doi:10.1007/s00410-009-0478-2

Shu, L. S., Deng, P., Wang, B., Tan, Z. Z., Yu, X. Q., and Sun, Y. (2004). Lithology, kinematics and geochronology related to Late Mesozoic basin-mountain evolution in the Nanxiong-Zhuguang area, South China. *Sci. China Ser. D-Earth Sci.* 47 (8), 673–688. doi:10.1360/03yd0113

Singsoupho, S., Bhongsuwan, T., and Elming, S. A. (2014). Tectonic evaluation of the Indochina Block during Jurassic-Cretaceous from palaeomagnetic results of Mesozoic redbeds in central and southern Lao PDR. *J. Asian Earth Sci.* 92, 18–35. doi:10.1016/j.jseaes.2014.06.001

Stern, R. J., Tamura, Y., Masuda, H., Fryer, P., Martinez, F., Ishizuka, O., et al. (2013). How the Mariana volcanic arc ends in the south. *Isl. Arc.* 22 (1), 133–148. doi:10.1111/iar.12008

Stern, R. J., Tamura, Y., Shukuno, H., and Miyazaki, T. (2019). The zealandia volcanic complex: further evidence of a lower crustal "hot zone" beneath the Mariana intra-oceanic arc, western pacific. *Isl. Arc.* 28, e12308. doi:10.1111/iar.12308

Sun, L. Q., Ling, H. F., Zhao, K. D., Chen, P. R., Chen, W. F., Sun, T., et al. (2017). Petrogenesis of early cretaceous adakitic granodiorite: implication for a crust thickening event within the cathaysia block, south China. *Sci. China-Earth Sci.* 60, 1237–1255. doi:10.1007/s11430-016-5200-y

Sun, S. J., Zhang, L. P., Zhang, R. Q., Ding, X., Zhu, H. L., Zhang, Z. F., et al. (2018). Mid-late cretaceous igneous activity in south China: the Qianjia example, hainan island. *Int. Geol. Rev.* 60 (11-14), 1665–1683. doi:10.1080/00206814.2017.1402379

Sun, S. S., and McDonough, W. F. (1989). Chemical and isotopic systematics of oceanic basalts: implications for mantle composition and processes. *Geol. Soc. Lond. Spec. Publ.* 42 (1), 313–345. doi:10.1144/gsl.sp.1989.042.01.19

Sun, W. (2016). Initiation and evolution of the South China sea: an overview. *Acta Geochim.* 35, 215–225. doi:10.1007/s11631-016-0110-x

Tang, G. J., and Wang, Q. (2010). High-Mg andesites and their geodynamic implications. *Acta Petrol. Sin.* 26 (8), 2495–2512.

Tang, L., Chen, H., and Dong, C. (2014). Zircon U-Pb dating and Tectonic significance of late Mesozoic granodiorite and its enclaves from Hainan Island. *Chin. J. Geol.* 49 (1), 259–274. doi:10.3969/j.issn.0563-5020.2014.01.019

Tang, L. M., Chen, H. L., Dong, C. W., Shen, Z. Y., Cheng, X. G., and Fu, L. L. (2010). Late mesozoic tectonic extension in SE China: evidence from the basic dike swarms in hainan island, China. *Acta Petrol. Sin.* 26 (4), 1204–1216.

Tapponnier, P., Peltzer, G., Le Dain, A. Y., Armijo, R., and Cobbold, P. (1982). Propagating extrusion tectonics in Asia: new insights from simple experiments with plasticine. *Geology* 10 (12), 611. doi:10.1130/0091-7613(1982)10<611:petian>2.0.co;2

Tatsumi, Y. (2001). Geochemical modeling of partial melting of subducting sediments and subsequent melt-mantle interaction: generation of high-Mg andesites in the setouchi volcanic belt, southwest Japan. *Geology* 29 (4), 323–326. doi:10.1130/0091-7613(2001)029<0323:GMOPMO>2.0.CO;2

Tatsumi, Y. (2006). High-Mg andesites in the setouchi volcanic belt, southwestern Japan: analogy to archean magmatism and continental crust formation? *Annu. Rev. Earth Planet. Sci.* 34, 467–499. doi:10.1146/annurev.earth.34.031405.125014

Thuy, N. T. B., Satir, M., Siebel, W., Vennemann, T., and Long, T. V. (2004). Geochemical and isotopic constraints on the petrogenesis of granitoids from the Dalat zone, southern Vietnam. *J. Asian Earth Sci.* 23, 467–482. doi:10.1016/j.jseaes.2003.06.001

Tormey, D. R., Frey, F. A., and Lopez-Escobar, L. (1995). Geochemistry of the active azufre-planchon-peteroa volcanic complex, Chile (35°15′S): evidence for multiple sources and processes in a cordilleran arc magmatic system. *J. Petrol.* 36 (2), 265–298. doi:10.1093/petrology/36.2.265

Wade, J. A., Plank, T., Stern, R. J., Tollstrup, D. L., Gill, J. B., O'Leary, J. C., et al. (2005). The may 2003 eruption of anatahan volcano, Mariana islands: geochemical evolution of a silicic island-arc volcano. *J. Volcanol. Geotherm. Res.* 146 (1–3), 139–170. doi:10.1016/j.jvolgeores.2004.11.035

Wang, D. Z., Shu, L. S., Faure, M., and Sheng, W. Z. (2001). Mesozoic magmatism and granitic dome in the Wugongshan Massif, Jiangxi Province and their genetical relationship to the tectonic events in Southeast China. *Tectonophysics* 339, 259–277. doi:10.1016/s0040-1951(01)00130-5

Wang, Q., Li, X. H., Jia, X. H., Wyman, D., Tang, G. J., Li, Z. X., et al. (2012). Late early cretaceous adakitic granitoids and associated magnesian and potassium-rich mafic enclaves and dikes in the tunchang-fengmu area, hainan province (south China): partial melting of lower crust and mantle, and magma hybridization. *Chem. Geol.* 328, 222–243. doi:10.1016/j.chemgeo.2012.04.029

Wang, Q., Tang, G., Hao, L., Wyman, D., Ma, L., Dan, W., et al. (2020). Ridge subduction, magmatism, and metallogenesis. *Sci. China-Earth Sci.* 63 (10), 1499–1518. doi:10.1007/s11430-019-9619-9

Wang, T., Li, G., Wang, Q., Santosh, M., Zhang, Q., and Deng, J. (2019). Petrogenesis and metallogenic implications of Late Cretaceous I- and S-type granites in Dachang-Kunlunguan ore belt, southwestern South China Block. *Ore Geol. Rev.* 113, 103079. doi:10.1016/j.oregeorev.2019.103079

Watson, E. B., and Harrison, T. M. (1983). Zircon saturation revisited: temperature and composition effects in a variety of crustal magma types. *Earth Planet. Sci. Lett.* 64, 295–304. doi:10.1016/0012-821X(83)90211-X

Whalen, J. B., Currie, K. L., and Chappell, B. W. (1987). A-Type granites: geochemical characteristics, discrimination and petrogenesis. *Contrib. Mineral. Petrol.* 95, 407–419. doi:10.1007/BF00402202

Wong, J., Sun, M., Xing, G., Li, X., Zhao, G., Wong, K., et al. (2009). Geochemical and zircon U-Pb and Hf isotopic study of the baijuhuajian metaluminous A-type granite: extension at 125–100 Ma and its tectonic significance for south China. *Lithos* 112, 289–305. doi:10.1016/j.lithos.2009.03.009

Woodhead, J. D. (1989). Geochemistry of the Mariana Arc (western pacific): source composition and processes. *Chem. Geol.* 76 (1–2), 1–24. doi:10.1016/0009-2541(89)90124-1

Xia, S., and Zhao, D. (2014). Late mesozoic magmatic plumbing system in the onshore-offshore area of Hong Kong: insight from 3-D active-source seismic tomography. *J. Asian Earth Sci.* 96, 46–58. doi:10.1016/j.jseaes.2014.08.038

Xiao, E., Qiu, J. S., Xu, X. S., Jiang, S. Y., Hu, J., and Li, Z. (2007). Geochronology and geochemistry of the yaokeng alkaline granitic pluton in Zhejiang province: petrogenetic and tectonic implications. *Acta Petrol. Sin.* 23 (6), 1431–1440.

Xu, D. R., Wu, C. J., Hu, G. C., Chen, M. L., Fu, Y. R., Wang, Z. L., et al. (2016). Late mesozoic molybdenum mineralization on hainan island, south China: geochemistry, geochronology and geodynamic setting. *Ore Geol. Rev.* 72, 402–433. doi:10.1016/j.oregeorev.2015.07.023

Yan, L., He, Z., Beier, C., and Klemd, R. (2018). Geochemical constraints on the link between volcanism and plutonism at the Yunshan caldera complex, SE China. *Contrib. Mineral. Petrol.* 173, 4. doi:10.1007/s00410-017-1430-5

Yan, L. L., He, Z. Y., Jahn, B., and Zhao, Z. D. (2016). Formation of the Yandangshan volcanic-plutonic complex (SE China) by melt extraction and crystal accumulation. *Lithos* 266–267, 287–308. doi:10.1016/j.lithos.2016.10.029

Yan, Q., Metcalfe, I., and Shi, X. (2017). U-Pb isotope geochronology and geochemistry of granites from hainan island (northern south China sea margin):

constraints on late paleozoic-mesozoic tectonic evolution. *Gondwana Res.* 49, 333–349. doi:10.1016/j.gr.2017.06.007

Yan, Q., Shi, X., and Castillo, P. R. (2014). The late mesozoic-cenozoic tectonic evolution of the South China sea: A petrologic perspective. *J. Asian Earth Sci.* 85, 178–201. doi:10.1016/j.jseaes.2014.02.005

Yan, Q., Shi, X., Liu, J., Wang, K., and Bu, W. (2010). Petrology and geochemistry of mesozoic granitic rocks from the nansha micro-block, the South China sea: constraints on the basement nature. *J. Asian Earth Sci.* 37 (2), 130–139. doi:10.1016/j.jseaes.2009.08.001

Yang, G. X. (2022). Subduction initiation triggered by collision: A review based on examples and models. *Earth-Sci. Rev.* 232, 104129. doi:10.1016/j.earscirev.2022.104129

Ye, Q., Mei, L., Shi, H., Camanni, G., Shu, Y., Wu, J., et al. (2018). The late cretaceous tectonic evolution of the South China sea area: an overview, and new perspectives from 3D seismic reflection data. *Earth-Sci. Rev.* 187, 186–204. doi:10.1016/j.earscirev.2018.09.013

Yichang IGMR and Hainan GS (2004). *Regional geological survey report of 1: 250000 ledong County and lingshi county Sheet in hainan Province*. Yichang: Yichang IGMR.

Yin, A. (2010). Cenozoic tectonic evolution of Asia: A preliminary synthesis. *Tectonophysics* 488 (1-4), 293–325. doi:10.1016/j.tecto.2009.06.002

Yu, M. G., Xing, G. F., Shen, J. L., Chen, R., Zhou, Y. Z., Wei, H. M., et al. (2008). Volcanism of the yandang mountain world geopark. *Acta Petrologica Mineralogical* 27 (2), 101–112.

Yuan, X., Fang, N., Dong, H., and Shen, X. (2019). Comparison of surgical field visibility during propofol or desflurane anesthesia for middle ear microsurgery. *Geoscience* 33 (1), 85–97. doi:10.1186/s12871-019-0759-x

Zahirovic, S., Matthews, K. J., Flament, N., Müller, R. D., Hill, K. C., Seton, M., et al. (2016). Tectonic evolution and deep mantle structure of the eastern Tethys since the latest Jurassic. *Earth-Sci. Rev.* 162, 293–337. doi:10.1016/j.earscirev.2016.09.005

Zhang, L., Deng, J., Sun, S., Sui, Q., Wang, K., and Sun, W. (2023). Subduction of the neo-tethys ridge beneath the eurasian continent during the cretaceous. *Ore Geol. Rev.* 154, 105302. doi:10.1016/j.oregeorev.2023.105302

Zhang, L., Hu, Y., Liang, J., Ireland, T., Chen, Y., Zhang, R., et al. (2017). Adakitic rocks associated with the Shilu copper-molybdenum deposit in the Yangchun Basin, South China, and their tectonic implications. *Acta Geochim.* 36 (2), 132–150. doi:10.1007/s11631-017-0146-6

Zhang, L. L., Zhu, D. C., Wang, Q., Zhao, Z. D., Liu, D., and Xie, J. C. (2019a). Late cretaceous volcanic rocks in the sangri area, southern Lhasa Terrane, Tibet: evidence for oceanic ridge subduction. *Lithos* 326-327, 144–157. doi:10.1016/j.lithos.2018.12.023

Zhang, Z. M., Ding, H. X., Dong, X., and Tian, Z. L. (2019b). Formation and evolution of the Gangdese magmatic arc, southern Tibet. *Acta Petrol. Sin.* 35 (2), 275–294. doi:10.18654/1000-0569/2019.02.01

Zhao, X., Jiang, Y., Xing, G., Chen, Z., Liu, K., Yu, M., et al. (2018). A geochemical and geochronological study of the Early Cretaceous, extension-related Honggong ferroan (A-type) granite in southwestern Zhejiang Province, southeast China. *Geol. Mag.* 155 (3), 549–567. doi:10.1017/S0016756816000790

Zhou, X. M., and Li, W. X. (2000). Origin of late mesozoic igneous rocks in southeastern China: implications for lithosphere subduction and underplating of mafic magmas. *Tectonophysics* 326 (3–4), 269–287. doi:10.1016/s0040-1951(00)00120-7

Zhou, X., Sun, T., Shen, W., Shu, L., and Niu, Y. (2006). Petrogenesis of mesozoic granitoids and volcanic rocks in south China: A response to tectonic evolution. *Episodes* 29 (1), 26–33. doi:10.18814/epiiugs/2006/v29i1/004

Zhou, Y., Liang, X., Kröner, A., Cai, Y., Shao, Y., Wen, S., et al. (2015a). Late cretaceous lithospheric extension in SE China: constraints from volcanic rocks in hainan island. *Lithos* 232, 100–110. doi:10.1016/j.lithos.2015.06.028

Zhou, Y., Liang, X., Liang, X., Jiang, Y., Wang, C., Fu, J., et al. (2015b). U–Pb geochronology and Hf-isotopes on detrital zircons of lower paleozoic strata from hainan island: new clues for the early crustal evolution of southeastern south China. *Gondwana Res.* 27 (4), 1586–1598. doi:10.1016/j.gr.2014.01.015

Zhu, W. L., Xie, X. N., Wang, Z. F., Zhang, D. J., Zhang, C. L., Cao, L. C., et al. (2017). New insights on the origin of the basement of the Xisha uplift, south China sea. *Sci. China-Earth Sci.* 60 (12), 2214–2222. doi:10.1007/s11430-017-9089-9